

SAR COMPLIANCE TESTING OF WISTRON NEWEB MODEL EM-500AG 802.11 a/b/g  
MINI PCI BUILT INTO ACER MODEL MS2143 NOTEBOOK COMPUTER

FCC ID# NKRMS2143CM6

Host Computer: Acer Model MS2143  
S/N: 8143D0100133300C6AM000

December 9, 2003

Prepared for: Wistron NeWeb Corporation  
No. 10-1, Li-Hsin Road I  
Science-Based Industrial Park  
Hsinchu 300, Taiwan, R.O.C.

Prepared by: Om P. Gandhi  
Professor of Electrical and Computer Engineering  
University of Utah  
50 S Central Campus Dr., Rm. 3280  
Salt Lake City, UT 84112-9206

## TABLE OF CONTENTS

I.	Introduction .....	1
II.	The SAR Measurement System .....	2
	The Flat Phantom .....	3
III.	Calibration of the E-Field Probe .....	3
IV.	SAR System Verification .....	5
V.	Tissue Simulant Fluid for the Frequency Band 5.2 to 5.8 GHz .....	6
VI.	The Measured SAR Distributions .....	7
VII.	Comparison of the Data with FCC 96-326 Guidelines .....	9
	REFERENCES .....	10
	TABLES .....	12
	FIGURES .....	15
	APPENDIX A .....	31
	APPENDIX B .....	36
	APPENDIX C .....	40
	APPENDIX D .....	45
	APPENDIX E .....	61
	APPENDIX F .....	63
	APPENDIX G .....	75

SAR COMPLIANCE TESTING OF WISTRON NEWEB MODEL EM-500AG 802.11 a/b/g  
MINI PCI BUILT INTO ACER MODEL MS2143 NOTEBOOK COMPUTER

FCC ID# NKRMS2143CM6

Host Computer: Acer Model MS2143,  
S/N: 8143D0100133300C6AM000

## I. Introduction

We have used the measurement procedures outlined in FCC Supplement C (Edition 97-01) to OET Bulletin 65 [1] and an updated version of the same [2] for evaluating compliance of the Wistron NeWeb Model EM-500AG Mini PCI (FCC ID#NKRMS2143CM6) built into Acer Model MS2143 Notebook Computer. Three photographs of the Acer Model MS2143 Notebook Computer with Wistron NeWeb Model EM-500AG Mini PCI built in it are given in Figs. 1a-c, respectively. Given in Fig. 2 is a photograph of the Acer Model MS2143 Notebook Computer illustrating the locations of the right side "Main" antenna and left side "Aux" antenna, respectively. From Fig. 2, it can be seen that both the "Main" and "Aux" antennas are built close to the hinge areas of the display screen at distances of about 5.3 and 8.0 cm from the right and left edges of the PC, respectively. Furthermore, as seen from Fig. 1c, the edge of the display screen containing the two built-in antennas of the Mini PCI is recessed from the back edge of the base by about 1.4 cm.

The Wistron NeWeb Model EM-500AG Mini PCI 802.11a antennas operate over the frequency band 5.15-5.81 GHz in the normal and turbo modes with conducted powers that are given in Table 1.

For SAR measurements, three configurations of the wireless PC relative to the experimental phantom have been used. These are as follows:

- a. **Configuration 1** is for the wireless PC placed on a user's lap. For this configuration, a planar phantom model with inside dimensions 12"  $\times$  16.5" (30.5  $\times$  41.9 cm) and a base thickness of  $2.0 \pm 0.2$  mm (recommended in [2]) was used for SAR measurements and the bottom side of the laptop computer shown in Fig. 1b was pressed against it (see

Fig. 3a). For this configuration, the SARs were extremely low close to the noise level of the measuring system (estimated to be on the order of 0.02 W/kg) both for the Main and the Aux antennas of the Mini PCI (see Fig. 2). This is likely due to a physical separation on the order of 4 cm for both the Main and the Aux antennas to the base of the Acer Notebook Computer.

- b. **Configuration 2** – Edge-on position. This corresponds to a bystander standing next to right or left edges of the PC. For this configuration, the PC is placed at 90° with the right or the left edge of the PC pressed against the bottom of the planar phantom (see Fig. 3b for the left edge placement). Here too, since both of the antennas i.e. the Main and the Aux antennas are several centimeters away from the proximal edges, the SARs were too low to measure and within the noise level of the measuring system ( $\leq 0.02$  W/kg).
- c. **Configuration 3** – Edge-on position. This corresponds to the case of a bystander behind the PC screen with separation of 0 cm from the PC edge. This configuration was selected since the Main and the Aux antennas are built close to the back edge of the PC. For SAR measurement for this configuration, the PC was placed with the broader back edge of the host computer at 90° pressed against the bottom of the planar phantom with separation of 0 cm (see Fig. 4).

## II. The SAR Measurement System

The University of Utah SAR Measurement System has been described in peer-reviewed literature [3]. A photograph of the SAR Measurement System is given in Fig. 5. This SAR Measurement System uses a computer-controlled 3-D stepper motor system (Arrick Robotics MD-2A). A triaxial Narda Model 8021 E-field probe is used to determine the internal electric fields. The positioning repeatability of the stepper motor system moving the E-field probe is within  $\pm 0.1$  mm. Outputs from the three channels of the E-field probe are dc voltages, the sum of which is proportional to the square of the internal electric fields  $(|E_i|^2)$  from which the SAR can be obtained from the equation  $SAR = \sigma(|E_i|^2)/\rho$ , where  $\sigma$  and  $\rho$  are the conductivity and

mass density of the tissue-simulant materials, respectively [4]. The dc voltages for the three channels of the E-field probe are read by three HP 34401A multimeters and sent to the computer via an HPIB interface. The setup is carefully grounded and shielded to reduce the noise due to the electromagnetic interference (EMI). A cutout in a wooden table allows placement of a plastic holder (shown in Fig. 6) on which the laptop computer with the 802.11a wireless antennas (see Fig. 1) is supported. The plastic holder (see Fig. 6) can be moved up or down so that the base of the PC (for Configuration 1) is pressed against the base of the flat phantom for determination of SAR for Above-lap position (see Fig. 3a). Similarly, for "Edge-On" SAR determination, Configuration 2, the laptop computer is mounted sideways (at 90°) on the plastic holder and moved up so that the right or left edge is pressed against the bottom of the flat phantom (see Fig. 3b). A second bystander (Configuration 3) – the so-called End-on position, where an individual may be behind the PC screen at a distance of 0 cm from the broader back edge of the PC (see Fig. 4) was also used for SAR measurements.

#### *The Flat Phantom*

As recommended in Supplement C Edition 01-01 to OET Bulletin 65 [2], a planar phantom model with inside dimensions 12"  $\times$  16.5" (30.5  $\times$  41.9 cm) and base thickness  $2.0 \pm 0.2$  mm was used for SAR measurements (see Figs. 3 and 4).

### **III. Calibration of the E-Field Probe**

The IEEE Standard P1528 [5] suggests a recommended procedure for probe calibration (see Section 4.4.1 of [5]) for frequencies above 800 MHz where waveguide size is manageable. Calibration using an appropriate rectangular waveguide is recommended. As in some previously reported SAR measurements at 6 GHz [4], we have calibrated the Narda Model 8021 Miniature Broadband Electric Field Probe of tip diameter 4 mm (internal dipole dimensions on the order of 2.5 mm) using a rectangular waveguide WR 159 (of internal dimensions 1.59  $\times$  0.795 inches) that was filled with the tissue-simulant fluid of composition given in Section V (see Figs. 7a, b).

The triaxial (3 dipole) E-field probe shown in Fig. 8 was originally developed by Howard Bassen and colleagues of FDA and has been manufactured under license by Narda Microwave Corporation, Hauppauge, New York. The probe is described in detail in references 6 and 7. It uses three orthogonal pick up dipoles each of length about 2.5 mm offset from the tip by 3 mm, each with its own leadless zero voltage Schottky barrier diode operating in the square law region. The sum of the three diode outputs read by three microvoltmeters [3] gives an output proportional to  $E^2$ . By rotating the probe around its axis, the isotropy of the probe was measured to be less than  $\pm 0.23$  dB and the deviation of the probe from the square law behavior was less than  $\pm 3\%$ .

As suggested in the IEEE Standard P1528, the waveguide (WR 159) filled with the tissue-simulant fluid was maintained vertically. From microwave field theory [see e.g. ref. 8], the transverse field distribution in the liquid corresponds to the fundamental mode (TE<sub>10</sub>) with an exponential decay in the vertical direction (z-axis). The liquid level was 15 cm deep which is deep enough to guarantee that reflections from the top liquid surface do not affect the calibration. By comparing the square of the decaying electric fields expected in the tissue from the analytical expressions for the TE<sub>10</sub> mode of the rectangular waveguide, we obtained a calibration factor of 2.98 (mW/kg)/ $\mu$ V with a variability of less than  $\pm 2\%$  for measurement frequencies of 5.25 and 5.8 GHz, respectively. This is no doubt due to a fairly limited frequency band of only 0.55 GHz out of a recommended bandwidth of 2.2 GHz for the TE<sub>10</sub> mode for the WR159 waveguide (recommended band of 4.9-7.1 GHz -- see e.g. ref. 8) and the fact that the bandwidth of 550 MHz for the entire set of measurements is on the order of  $\pm 5\%$  of the midband frequencies.

The date for the calibration of the E-field probe closest to the SAR tests given here was December 5, 2003.

To verify that the probe calibration conducted for the 802.11a band with CW signals is also valid for modulated signals used for the Mini PCI, two procedures have been used. These are described in Appendix A.

#### IV. SAR System Verification

It is very difficult to develop half wave dipole antennas for use in the 5.2 to 5.8 GHz band both because of fairly small dimensions and the resulting dimensional tolerances, and relatively narrow bandwidths of the required baluns – balanced-to-unbalanced transformers. On the other hand, waveguides are broadband with simultaneous bandwidths larger than 1-2 GHz and fairly easy to use for frequencies in excess of 3 GHz. As shown in Fig. 9, we have, therefore, developed a system verification system by using an open-ended, air-filled waveguide as an irradiation system placed at a distance of 8 mm below the base of the planar phantom (10 mm from the lossy fluid in the phantom). For this application, we have set up a WR 187 rectangular waveguide of internal dimensions  $1.872'' \times 0.872''$  that is fed with microwave power from a Hewlett Packard Model 83620A Synthesized Sweeper (10 MHz-20 GHz). The operating ( $TE_{10}$  mode) band of this waveguide is from 3.95 to 5.85 GHz. The microwave circuit arrangement used for system verification is sketched in Fig. 10. When placed at a distance of 8 mm from the base of the planar phantom, the reflection coefficient is about 10-20%. As seen in Fig. 9, even this relatively small amount of reflection has been reduced to less than 0.5% by using a movable slide-screw waveguide tuner (Narda Model 22CI). The measured SAR distributions for peak 1-g SAR region using this system at 5.25 and 5.80 GHz for the day of the SAR measurements December 5, 2003, are given in Appendix B. Also given in Appendix B are the waveguide SAR plots for this date of SAR measurements. The peak 1-g SARs measured for 100 mW of radiated power for 5.25 and 5.80 GHz were 3.61 and 3.93 W/kg, respectively. The measured 1-g SARs are in excellent agreement with the FDTD-calculated 1-g SARs for this waveguide of 3.580 and 3.946 W/kg at 5.25 and 5.80 GHz, respectively. Also as expected, the measured SAR plots in Appendix B are quite symmetric at both of the irradiation frequencies.

For FDTD-calculations of the SAR distributions for the WR187 rectangular waveguide irradiation system, we have used the dielectric properties for the phantom given in Table 2 that have been taken from [2]. Using a resolution of 0.5 mm for the FDTD cells, the calculated variations of the SAR distributions are given in Figs. 11a, b as a function of height above the

bottom surface of the phantom. From Figs. 11a, b, it is obvious that the penetration of electromagnetic fields in the 5.2-5.8 GHz range is extremely shallow. The calculated depths of penetration corresponding to  $1/e^2$ -reduction of SAR (13.5% of the SAR at the surface) are only 6.85 and 5.95 mm at 5.25 and 5.8 GHz, respectively. Both of these depths of penetration for this near-field exposure system are very similar to those obtained for plane wave irradiation at these frequencies (7.15 mm for 5.25 GHz and 6.25 mm for 5.8 GHz).

Also shown in Figs. 11a, b are the SAR variations measured for this waveguide exposure system at depths of 4, 6, 8, 10, 12, and 14 mm in the tissue-simulant fluid. We tried second-, third-, fourth-, and fifth-order polynomial least-square fits to extrapolate the measured SARs to depths of 1, 3, 5, 7, and 9 mm. As seen in Figs. 11a, b, the fourth-order polynomial provides an excellent agreement with the FDTD-calculated in-depth variation of SAR both at 5.25 and 5.8 GHz. Also as aforementioned, the peak 1-g SARs thus obtained for 100 mW of radiated power for 5.25 and 5.80 GHz of 3.61 and 3.93 W/kg are extremely close to the FDTD-calculated 1-g SARs for this waveguide of 3.580 and 3.946 W/kg at the two frequencies, respectively.

## V. Tissue Simulant Fluid for the Frequency Band 5.2 to 5.8 GHz

In OET 65 Supplement C [2], the dielectric parameters suggested for body phantom are given only for 3000 and 5800 MHz. These are listed in Table 2 here. Using linear interpolation, we can obtain the dielectric parameters to use for the frequency band between 5.25 to 5.8 GHz. The desired dielectric properties thus obtained are also given in Table 2. From Table 2, it can be noticed that the desired dielectric constant  $\epsilon_r$  varies from 48.2 to 49.0 which is a variation of less than  $\pm 1\%$  from the average value of 48.6 for this band. Also the conductivity  $\sigma$  varies linearly with frequency from 5.36 to 6.00 S/m.

No tissue-simulant fluids have been suggested in any of the existing standards or draft standards [2, 5, 9, 10]. Because of this limitation, some of the standards are only written for frequencies up to 3 GHz [e.g. refs. 5, 9]. We have developed a fluid composition for which the measured dielectric properties for the 802.11a frequencies of 5.25 and 5.80 GHz are as follows:

For 5.25 GHz,

$$\epsilon_r = 49.6 \pm 0.6$$

$$\sigma = 5.35 \pm 0.09 \text{ S/m}$$

For 5.8 GHz,

$$\epsilon_r = 49.3 \pm 0.6$$

$$\sigma = 6.01 \pm 0.1 \text{ S/m}$$

The measurements of the dielectric properties ( $\epsilon'$ ,  $\epsilon''$ ) for this fluid composition were conducted using Hewlett Packard Model 85070B Dielectric Probe and the latest software 85070d provided by Agilent Technologies. The measured data is based on 11 repeated measurements of which five representative screen dumps are given in Appendix C, Figs. C.1-C.5, respectively. For each of the cases, the conductivity  $\sigma$  for the fluid may be obtained by multiplying  $\epsilon''$  by  $\omega\epsilon_0$  where  $\omega = 2\pi f$  and  $\epsilon_0$  is the permittivity of free space,  $8.854 \times 10^{-12} \text{ F/m}$ . The measured values of  $\epsilon_r$  and  $\sigma$  given above are extremely close to the suggested values given in Table 2:  $\epsilon_r = 48.9$ ,  $\sigma = 5.36 \text{ S/m}$  for 5.25 GHz and  $\epsilon_r = 48.2$  and  $\sigma = 6.00 \text{ S/m}$  for 5.80 GHz.

## VI. The Measured SAR Distributions

The RF power outputs measured for the Acer Model MS2143 PC for the normal and turbo modes used with this PC are given in Table 1. For SAR measurements, we selected frequencies of 5.26, 5.745, and 5.805 GHz for the normal mode and 5.25, 5.76, and 5.80 GHz for the turbo mode. The various frequencies were selected both for their highest power outputs as well as to cover the different frequency bands planned for this PC. As recommended in Supplement C, Edition 01-01 [2], the stability of the conducted power was determined by repeated SAR measurements at the same location for each of the selected channels. The variability of the SAR thus determined for three repeated measurements over a 60-minute time period was within  $\pm 0.1 \text{ dB}$  ( $\pm 2.5\%$ ).

The highest SAR region for each of the measurement frequencies was identified in the first instance by using a coarser sampling with a step size of 8.0 mm over three overlapping areas for a total scan area of  $11.2 \times 19.2$  cm. The data thus obtained was resolved into a  $4 \times 4$  times larger grid i.e. a grid involving  $56 \times 96$  points by linear interpolation using a 2 mm step size. After thus identifying the region of the highest SAR, the SAR distribution was then measured with a resolution of 2 mm in order to obtain the peak  $1 \text{ cm}^3$  or 1-g SAR. The SAR measurements were performed at 4, 6, 8, 10, 12 mm height from the bottom surface of the body-simulant fluid. The SARs thus measured were extrapolated using a fourth-order least-square fit to the measured data to obtain the SAR variation correctly for the 802.11a frequencies of 5.2 to 5.8 GHz [11, attached as Appendix D]. This allowed us to obtain SAR values at 1, 3, 5, 7 and 9 mm height that were used to obtain 1-g SARs. The uncertainty analysis of the University of Utah SAR measurement system is given in Appendix E. The combined standard uncertainty is  $\pm 8.3\%$ .

Since the PIFA antennas used for the "Main" and "Aux" antennas are built close to the hinge areas of the display screen, they are about 4 cm from the base of the PC. Also, the "Main" and "Aux" antenna are 5.3 and 8.0 cms from the right and left side edges of the PC, respectively (see Fig. 2). A net result of this physical separation on the order of several centimeters is that for Configurations 1 and 2 i.e. for the lap-top and edge placements of the PC, the SARs are very low and within the noise limit of the SAR measurement system ( $\leq 0.02 \text{ W/kg}$ ). Even for Configuration 3 – the so-called end placement shown in Fig. 4, the SARs are too low to measure for the left side "Aux" antenna, and significant and measurable only for the right side "Main" antenna. For the right side "Main" antenna, the coarse scans for the highest SAR regions for Configuration 3 (End-on position) are given in Appendix F, Figs. F.1 to F.6. In these figures, the two axes are marked in units of step size of 8 mm. Also shown in these figures are "Main" antenna outline overlaid on the SAR contours. Also given in Appendix F as Tables F.1 to F.6 are the SAR distributions for the peak SAR region of volume  $10 \times 10 \times 10$  mm for which the coarse scans are given in Figs. F.1 to F.6, respectively. The SARs are given for xy planes at

heights  $Z$  of 1, 3, 5, 7, and 9 mm from the bottom of the flat phantom. The individual SAR values for this grid of  $5 \times 5 \times 5$  or 125 points are averaged to obtain peak 1-g SAR values (for a volume of 1 cm<sup>3</sup>). The temperature variation of the tissue-simulant fluid measured with a Bailey Instruments Model BAT 8 Temperature Probe for measurements at the various frequencies was  $22.8 \pm 0.2^\circ\text{C}$ .

The z-axis scan plots taken at the highest SAR locations for each set of tests are given in Appendix G. As discussed in Section IV, the SARs drop off fairly rapidly with depth in the phantom.

The SAR measurement results for the Wistron NeWeb Model EM-500AG 802.11a Mini PCI built into Acer Model MS2143 Notebook Computer are summarized in Table 3. All of the measured 1-g SARs are less than the FCC 96-326 guideline of 1.6 W/kg.

## **VII. Comparison of the Data with FCC 96-326 Guidelines**

According to the FCC 96-326 Guideline, the peak SAR for any 1-g of tissue should not exceed 1.6 W/kg. For the Wistron NeWeb Model EM-500AG 802.11a Mini PCI built into Acer Model MS2143 Notebook Computer (FCC ID# NKRMS2143CM6), the measured peak 1-g SARs vary from 0 to 0.173 W/kg which are smaller than 1.6 W/kg.

## REFERENCES

1. K. Chan, R. F. Cleveland, Jr., and D. L. Means, "Evaluating Compliance With FCC Guidelines for Human Exposure to Radiofrequency Electromagnetic Fields," Supplement C (Edition 97-01) to OET Bulletin 65, December, 1997. Available from Office of Engineering and Technology, Federal Communications Commission, Washington D.C., 20554.
2. Federal Communications Commission "Supplement C Edition 01-01 to OET Bulletin 65 Edition 97-01" June 2001.
3. Q. Yu, O. P. Gandhi, M. Aronsson, and D. Wu, "An Automated SAR Measurement System for Compliance Testing of Personal Wireless Devices," *IEEE Transactions on Electromagnetic Compatibility*, Vol. 41(3), pp. 234-245, August 1999.
4. O. P. Gandhi and J-Y. Chen, "Electromagnetic Absorption in the Human Head from Experimental 6-GHz Handheld Transceivers," *IEEE Transactions on Electromagnetic Compatibility*, Vol. 39(4), pp. 547-558, 1995.
5. IEEE Standard P1528, "Recommended Practice for Determining the Peak Spatial-Average Specific Absorption Rate (SAR) in the Human Body Due to Wireless Communication Devices: Experimental Techniques," 2003.
6. H. Bassen, M. Swicord, and J. Abita, "A Miniature Broadband Electric Field Probe," Ann. New York Academy of Sciences, Vol. 247, pp. 481-493, 1974.
7. H. Bassen and T. Babij, "Experimental Techniques and Instrumentation," Chapter 7 in *Biological Effects and Medical Applications of Electromagnetic Energy*, O. P. Gandhi, Editor, Prentice Hall Inc., Englewood Cliffs, NJ, 1990.
8. O. P. Gandhi, *Microwave Engineering and Applications*, Pergamon Press, New York, 1981.
9. European Standard EN50361, "Basic Standard for the Measurement of Specific Absorption Rate Related to Human Exposure to Electromagnetic Fields from Mobile Phones (300 MHz-3 GHz)," CENELEC, Central Secretariat: rue de Stassart 35, B-1050, Brussels.
10. Draft IEC PT62209 Part 2, "Procedure to Measure the Specific Absorption Rate (SAR) for Two-Way Radios, Palmtop Terminals, Laptop Terminals, Desktop Terminals, and Body-Mounted Devices Including Accessories and Multiple Transmitters (30 MHz to 6 GHz)," Draft version 0.6.
11. Q. Li, O. P. Gandhi, and G. Kang, "An Open-Ended Waveguide System for SAR System Validation and/or Probe Calibration for Frequencies above 3 GHz," submitted for publication to *IEEE Transactions on Microwave Theory and Techniques*, June 2003 (attached here as Appendix D).

12. G. Kang and O. P. Gandhi, "Effect of Dielectric Properties on the Peak 1- and 10-g SAR for 802.11 a/b/g Frequencies 2.45 and 5.15 to 5.85 GHz," accepted for publication in *IEEE Transactions on Electromagnetic Compatibility*).

Table 1. Peak conducted RF power outputs measured at various frequencies for both the "Main" and "Aux" antennas of the Wistron NeWeb Model EM-500AG 802.11a/b/g Mini PCI built into Acer Model MS2143 Notebook Computer.

Channel	Frequency MHz	Peak Conducted RF Power (dBm)
Normal Mode		
1	5180	16.4
4	5240	16.5
5	5260	17.5
8	5320	16.8
9	5745	19.8
12	5805	20.6
Turbo Mode		
1	5210	15.0
2	5250	16.5
3	5290	16.2
4	5760	17.8
5	5800	19.6

Table 2. Dielectric parameters for body phantom for the frequency band 5.2 to 5.8 GHz [2].

Frequency (GHz)	$\epsilon_r$	$\sigma$ (S/m)	Reference
3.0	52.0	2.73	Ref. 2
	48.2	6.00	
5.25	48.9	5.36	Interpolated
	48.9	5.42	Interpolated
	48.7	5.53	Interpolated
	48.5	5.77	Interpolated
	48.3	5.88	Interpolated

Table 3. The SAR measurement results for the normal and turbo modes for both the "Main" and "Aux" antennas of the Wistron NeWeb Model EM-500AG Mini PCI built into Acer Model MS2143 Notebook Computer.

Liquid temperature =  $22.8 \pm 0.2^\circ\text{C}$   
 Measurement date: December 5, 2003

Config- uration	Separation from Phantom (cm)	Antenna	Mode	Fre- quency GHz	Conducted RF Output Power (dBm)		1-g SAR W/kg	See App. F Table	See App. F Figure
					Before	After			
1 Above- lap	0	Main	Normal	5.26	17.50	17.53	<0.02*	--	--
	0	Main	Normal	5.745	19.80	19.78	<0.02*	--	--
	0	Main	Normal	5.805	20.60	20.63	<0.02*	--	--
	0	Aux	Normal	5.26	17.50	17.47	<0.02*	--	--
	0	Aux	Normal	5.745	19.80	19.81	<0.02*	--	--
	0	Aux	Normal	5.805	20.60	20.64	<0.02*	--	--
	0	Main	Turbo	5.25	16.50	16.54	<0.02*	--	--
	0	Main	Turbo	5.76	17.80	17.73	<0.02*	--	--
	0	Main	Turbo	5.80	19.60	19.59	<0.02*	--	--
	0	Aux	Turbo	5.25	16.50	16.53	<0.02*	--	--
	0	Aux	Turbo	5.76	17.80	17.82	<0.02*	--	--
	0	Aux	Turbo	5.80	19.60	19.62	<0.02*	--	--
2 Edge- on	0	Main	Normal	5.26	17.50	17.45	<0.02*	--	--
	0	Main	Normal	5.745	19.80	19.84	<0.02*	--	--
	0	Main	Normal	5.805	20.60	20.62	<0.02*	--	--
	0	Aux	Normal	5.26	17.50	17.54	<0.02*	--	--
	0	Aux	Normal	5.745	19.80	19.77	<0.02*	--	--
	0	Aux	Normal	5.805	20.60	20.66	<0.02*	--	--
	0	Main	Turbo	5.25	16.50	16.51	<0.02*	--	--
	0	Main	Turbo	5.76	17.80	17.85	<0.02*	--	--
	0	Main	Turbo	5.80	19.60	19.63	<0.02*	--	--
	0	Aux	Turbo	5.25	16.50	16.48	<0.02*	--	--
	0	Aux	Turbo	5.76	17.80	17.82	<0.02*	--	--
	0	Aux	Turbo	5.80	19.60	19.61	<0.02*	--	--
3 End- on	0	Main	Normal	5.26	17.50	17.48	0.173	F-1	F-1
	0	Main	Normal	5.745	19.80	19.82	0.112	F-2	F-2
	0	Main	Normal	5.805	20.60	20.57	0.089	F-3	F-3
	0	Aux	Normal	5.26	17.50	17.46	<0.02*	--	--
	0	Aux	Normal	5.745	19.80	19.77	<0.02*	--	--
	0	Aux	Normal	5.805	20.60	20.57	<0.02*	--	--
	0	Main	Turbo	5.25	16.50	16.48	0.129	F-4	F-4
	0	Main	Turbo	5.76	17.80	17.84	0.114	F-5	F-5
	0	Main	Turbo	5.80	19.60	19.62	0.127	F-6	F-6
	0	Aux	Turbo	5.25	16.50	16.52	<0.02*	--	--
	0	Aux	Turbo	5.76	17.80	17.83	<0.02*	--	--
	0	Aux	Turbo	5.80	19.60	19.59	<0.02*	--	--

\* Too low to measure, within the noise level of the SAR measurement system.



a. Top cover with screen open.

Fig. 1. Photograph of the Wistron NeWeb Model EM-500AG Mini PCI built into Acer Model MS2143 Notebook Computer.



b. View from the bottom side of the laptop computer.

Fig. 1. Photograph of the Wistron NeWeb Model EM-500AG Mini PCI built into Acer Model MS2143 Notebook Computer.



- c. View from the top of the laptop computer. Note that the edge of the display screen containing the two built-in antennas is recessed from the back edge of the base by about 1.4 cm.

Fig. 1. Photograph of the Wistron NeWeb Model EM-500AG Mini PCI built into Acer Model MS2143 Notebook Computer.



Fig. 2. Photograph of the Acer Model MS2143 Notebook Computer illustrating the location of the right-side "Main" antenna and the left-side "Aux" antenna of the Wistron NeWeb Model EM-500 AG Mini PCI. Note that both the Main and Aux antennas are built close to the hinge areas of the display screen and this edge is recessed from the back edge of the base of the PC (see Fig. 1c).



Fig. 3a. Photograph of the bottom of the Acer Model MS2143 Notebook Computer pressed against the base of the planar phantom. This is **Configuration 1** – Laptop position for SAR testing.



Fig. 3b. Photograph of the Acer Model MS2143 NoteBook Computer with left edge of the PC at 90° pressed against the base of the planar phantom. This is **Configuration 2** for SAR testing and represents the case of a bystander in contact (at a distance of 0 cm) with the left edge of the PC.



Fig. 4. Photograph of the Acer Model MS2143 Notebook Computer with the broader back edge of the PC at 90° pressed against the bottom of the planar phantom with separation of 0 cm. This is **Configuration 3** for SAR testing and represents the case of a bystander behind the PC screen with a separation of 0 cm.

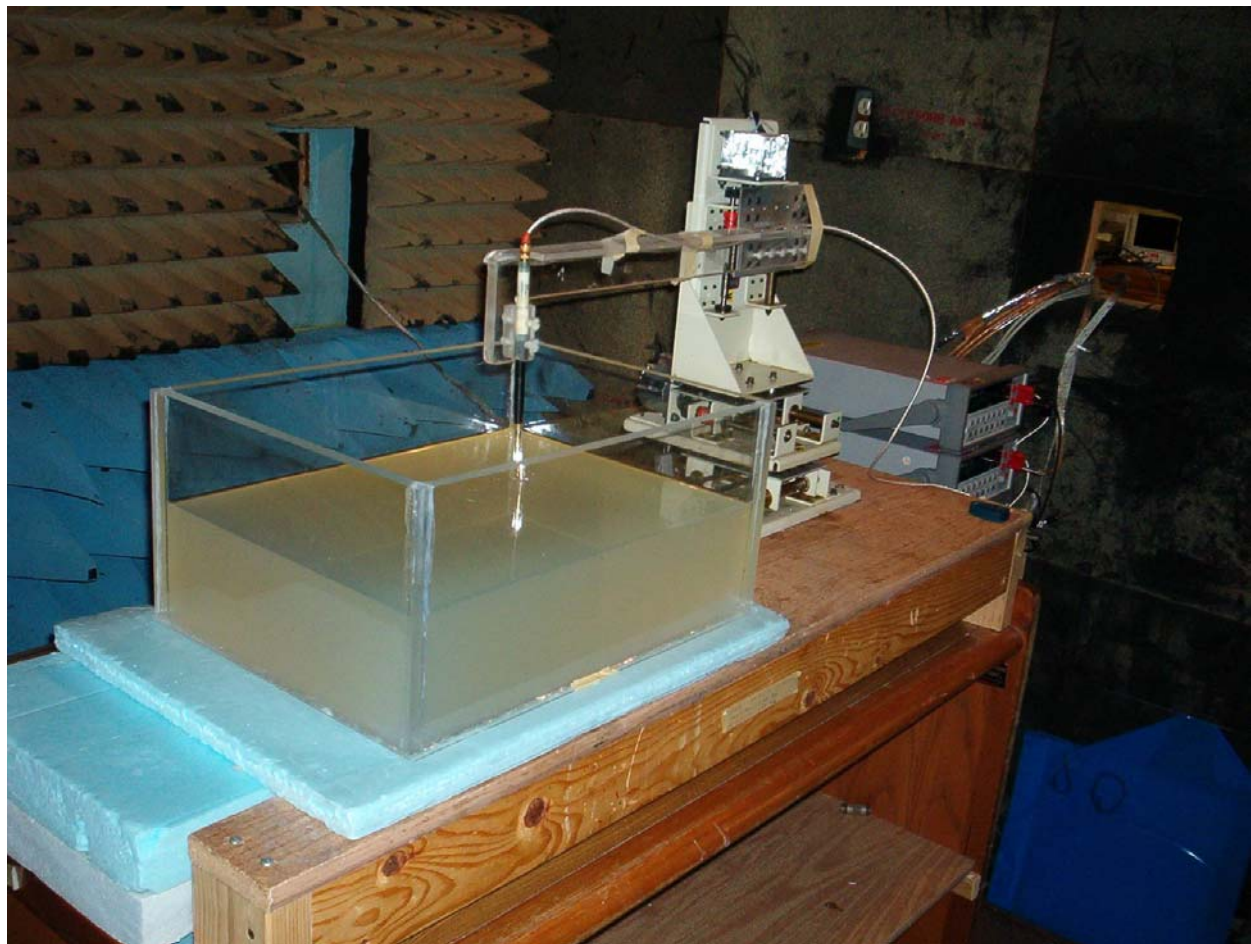


Fig. 5. Photograph of the three-dimensional stepper-motor-controlled SAR measurement system using a planar phantom.

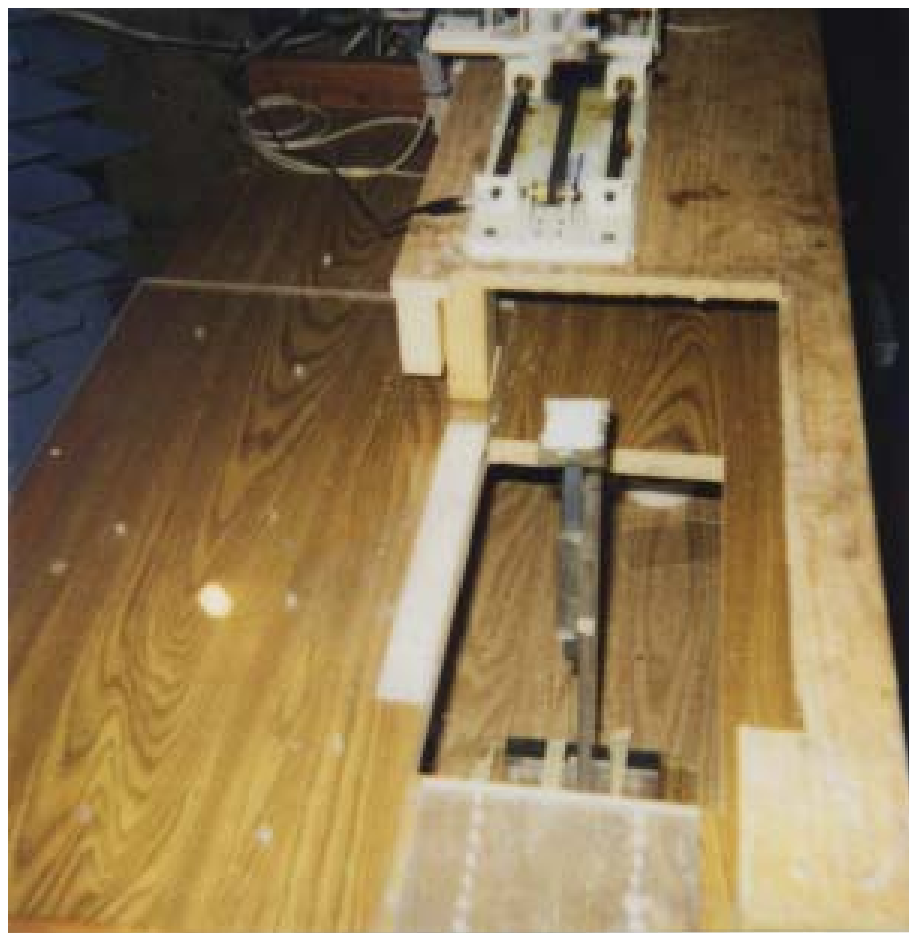


Fig. 6. The plastic holder used to support the portable PC for SAR measurements.

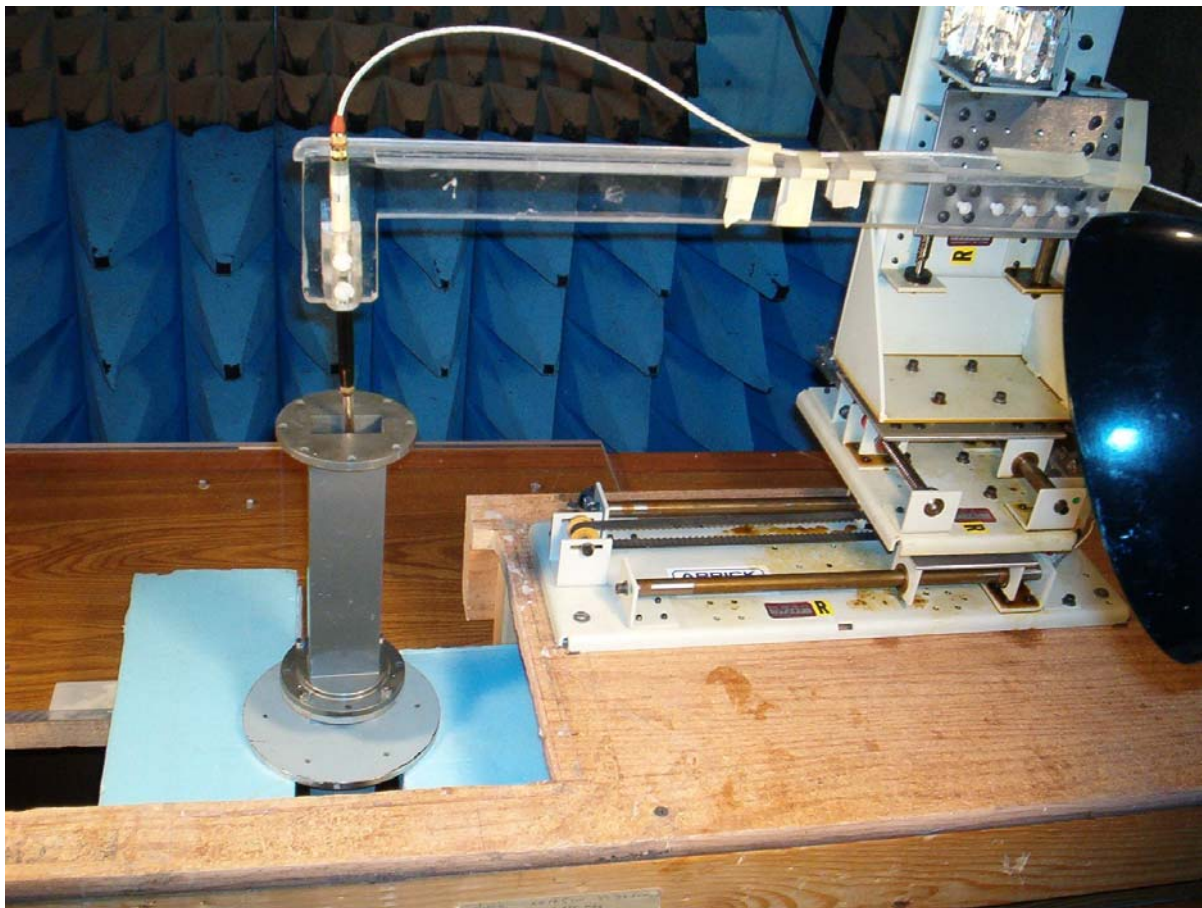


Fig. 7a. A photograph of the waveguide setup used for calibration of the Narda Model 8021 E-field probe in the frequency band 5.2-5.8 GHz.

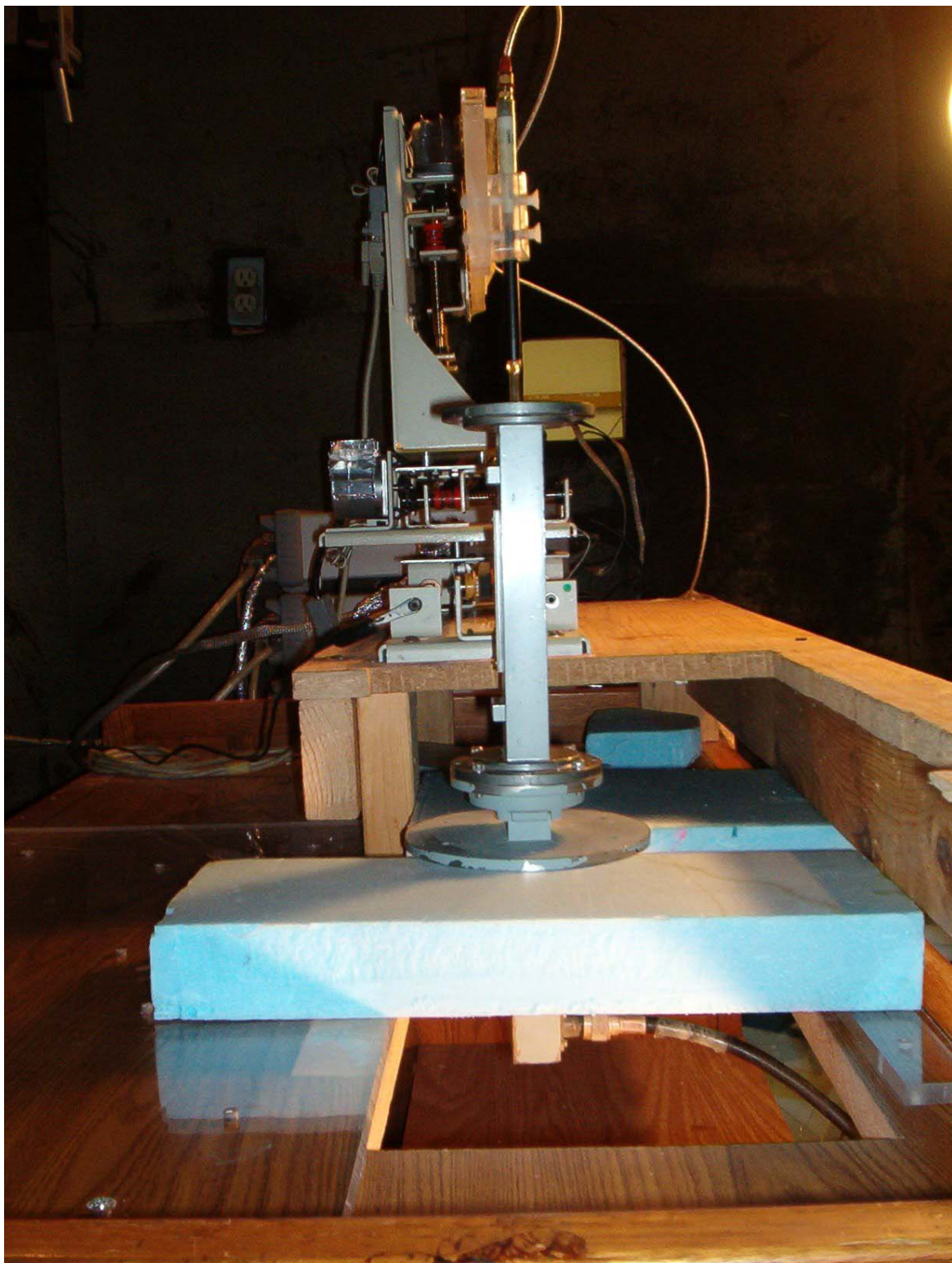


Fig. 7b. Photograph of the waveguide setup showing also the coax to waveguide coupler at the bottom used to feed power to the vertical waveguide containing the tissue-simulant fluid.



Fig. 8. Photograph of the Narda Model 8021 Broadband Electric Field Probe used for SAR measurements.

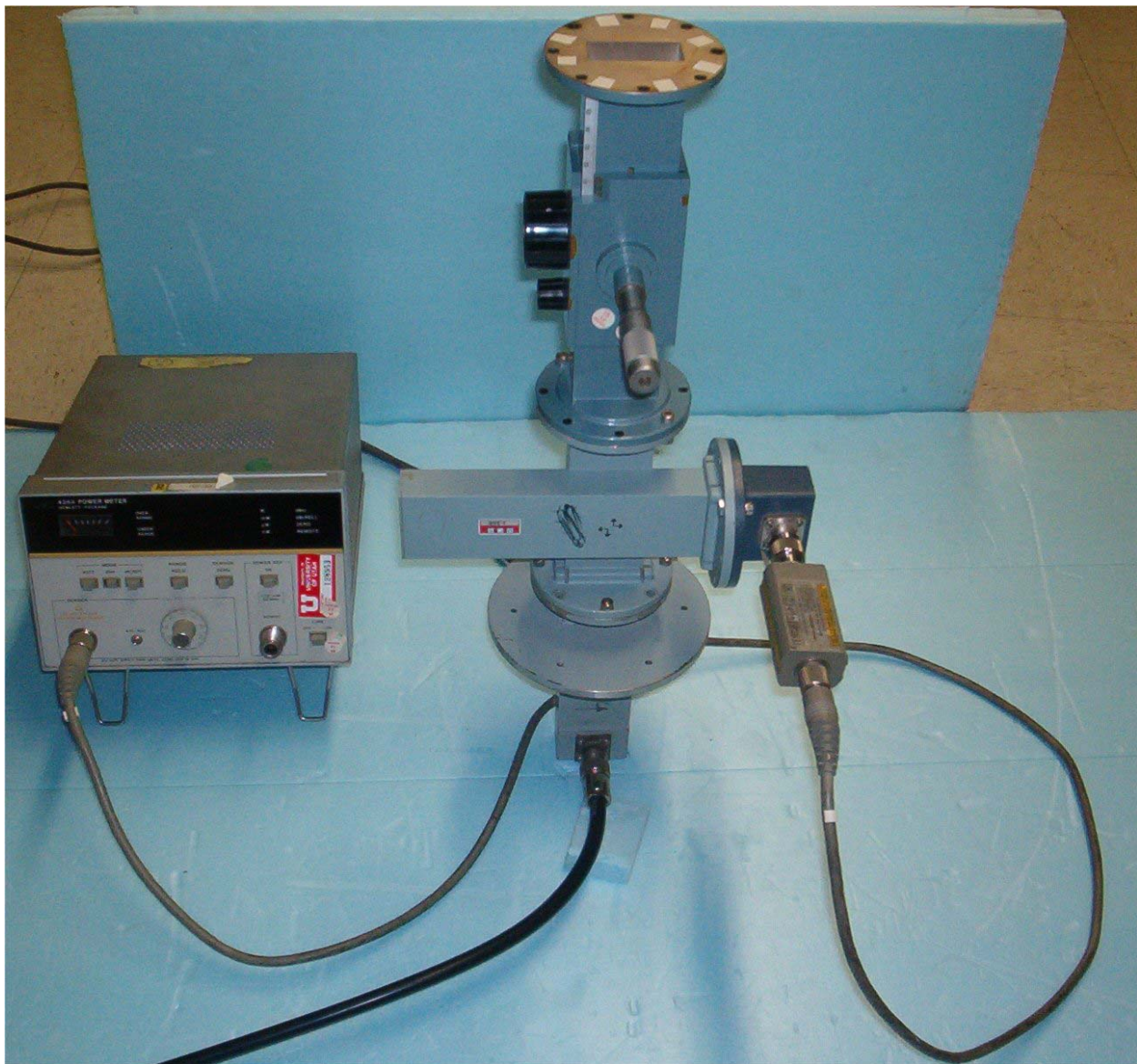
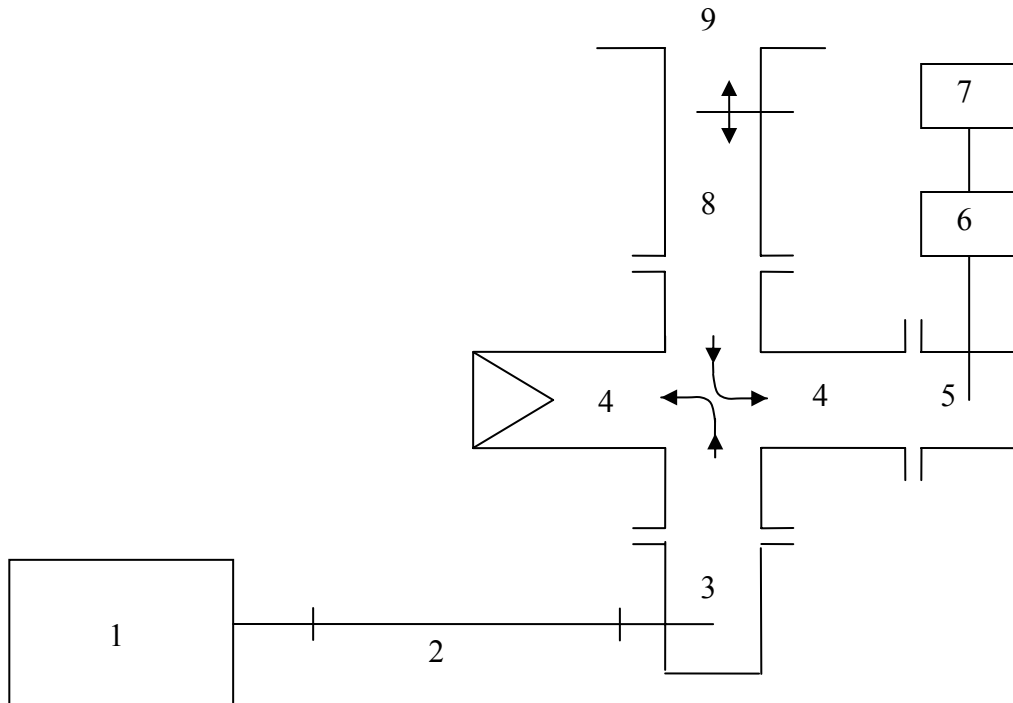
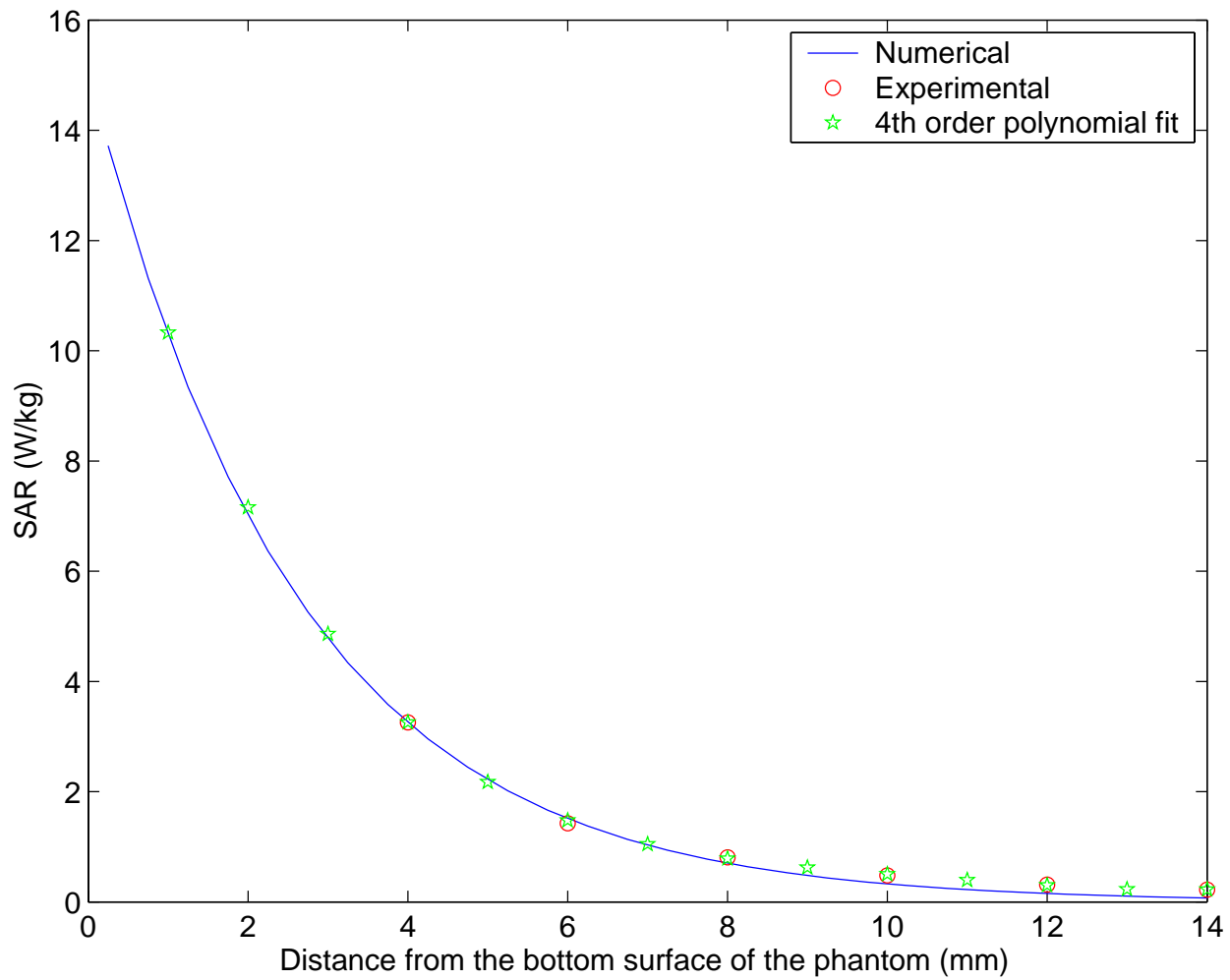


Fig. 9. Photograph of the rectangular waveguide radiator used for system verification for the 802.11a band. Also seen is the Narda Model 22CI movable slide screw tuner used to match the input power at 5.25 or 5.8 GHz to the planar phantom.



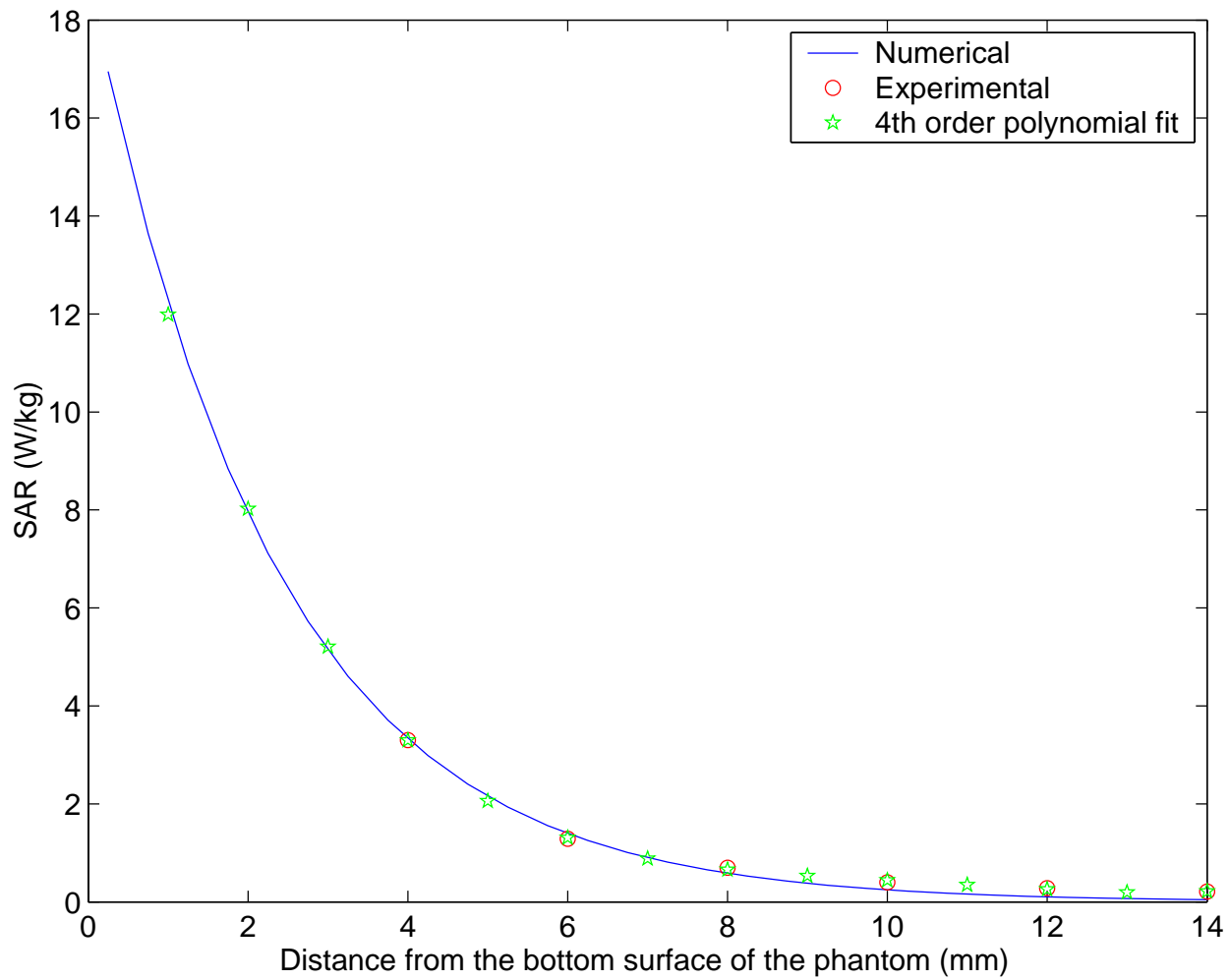
1. Hewlett Packard (HP) Model 83620A Synthesized Sweeper (10 MHz-20 GHz).
2. Coaxial line.
3. Coaxial to waveguide adapter.
4. 20 dB crossguide coupler (may be reversed to measure incident power).
5. HP Model G281A coaxial to waveguide adapter
6. HP Model 8482A power sensor.
7. HP Model 436A power meter.
8. Narda Microline® Slide Screw Tuner Model 22CI.
9. Radiating open end of the waveguide.

Fig. 10. The microwave circuit arrangement used for SAR system verification for the 802.11a band.



a. 5.25 GHz.

Fig. 11. Experimentally measured, extrapolated and FDTD-calculated variation of the SAR with depth in the body-simulant planar phantom. Radiated power = 100 mW.



b. 5.80 GHz.

Fig. 11. Experimentally measured, extrapolated and FDTD-calculated variation of the SAR with depth in the body-simulant planar phantom. Radiated power = 100 mW.

## APPENDIX A

### Procedures to Demonstrate that E-Field Probe Calibration for CW Signals is Also Valid for Modulated Signals

#### Procedure 1

For the microvoltmeters in our SAR system (HP34401 multimeters), we use an AC signal filter with a passband of 20 Hz to 300 kHz (1 reading/second). This allows faithful readings of the rectified values of voltage outputs from the three pickup antennas (proportional to  $E^2$ ) of the E-field probe used for SAR measurements. For a variety of modulated signals used for the 802.11a band, the multimeter passband of 20 Hz to 300 kHz is more than sufficient to read all of the frequency components. We have tested the validity of using this AC signal filter by applying signals from a Hewlett Packard Model 83620A Synthesized Sweeper operating at 5.25 and 5.8 GHz in the CW mode as well as the pulse mode with pulse repetition rates for the latter variable from 50 to 500 Hz and pulse duration variable from 0.5 to 1 msec. For a fixed location of the E-field probe, the SAR readings were proportional to the time-averaged radiated power (from 2.5 to 100 mW) from the WR187 rectangular waveguide at 5.25 and 5.8 GHz, respectively. Thus the probe calibration factors are no different for CW signals or for pulsed signals.

#### Procedure 2

As explained above, the passband of our SAR measurement system extends from 20 Hz to 300 kHz. This passband is more than sufficient to read all of the frequency components associated with OFDM or any of the other modulations that may be used for the 802.11a band.

Additional experiments have, however, been done to compare the SAR measured at one of the points in the planar phantom for OFDM modulated signals from the 802.11a Mini PCI and comparing the same with the CW signal of similar time-averaged power levels obtained from the Hewlett-Packard (HP) Model 83620A Synthesized Sweeper (10 MHz-20 GHz). For each of the two RF sources, the power output was measured using a microwave circuit arrangement similar to that of Fig. 10 of the SAR Report. As shown in this figure, the irradiation system uses a

WR187 rectangular waveguide (see Fig. 9 of the SAR Report) which is placed at a distance of 8 mm below the base of the planar phantom (10 mm from the lossy fluid in the phantom) used for SAR measurements.

Shown in Figs. A.1 and A.4 is a comparison of the SARs measured for a given location in the planar phantom for CW and 802.11a band modulated signals for the base and turbo modes, for several frequencies of the 802.11a band, respectively. An excellent agreement in the SAR reading is observed whether CW or modulated signals are used. This is due to the broad bandwidth (20 Hz to 300 kHz) of the system used for measuring rectified signals from the E-field probe.

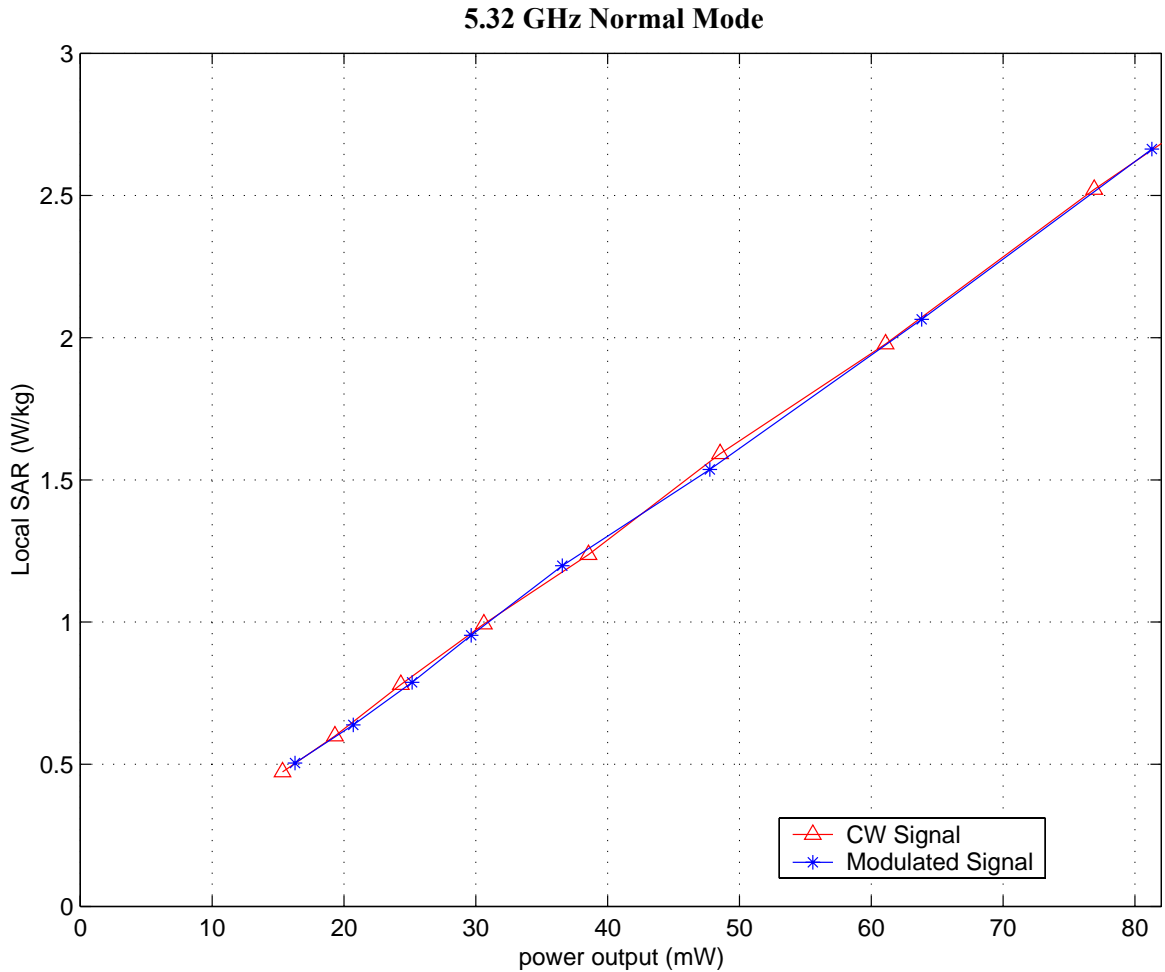


Fig. A.1. Comparison of the SAR for CW or OFDM modulated signals for the base mode at 5.32 GHz.

### 5.765 GHz Normal Mode

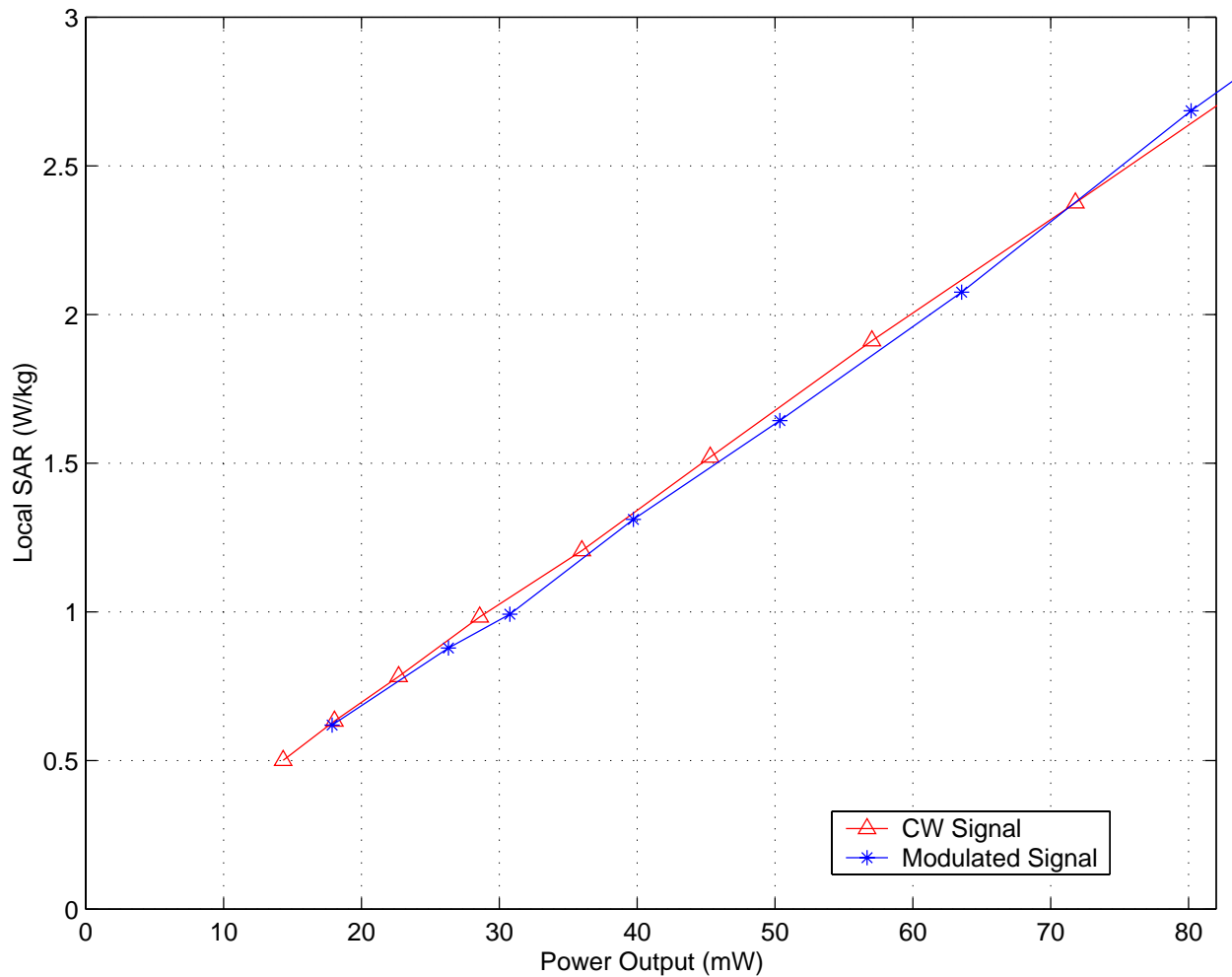


Fig. A.2. Comparison of the SAR for CW or OFDM modulated signals for the normal mode at 5.765 GHz.

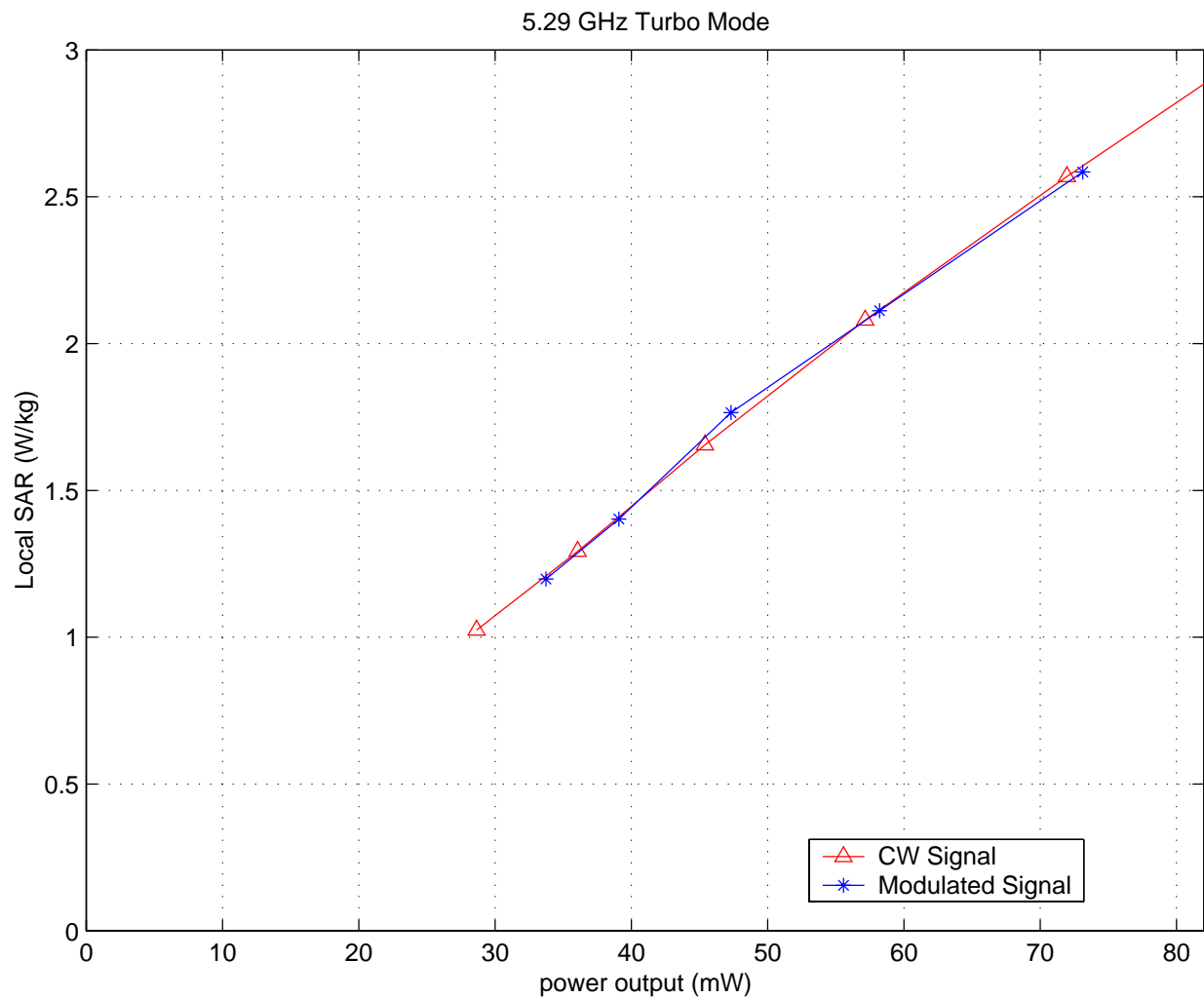


Fig. A.3. Comparison of the SAR for CW or OFDM modulated signals for the turbo mode at 5.29 GHz.

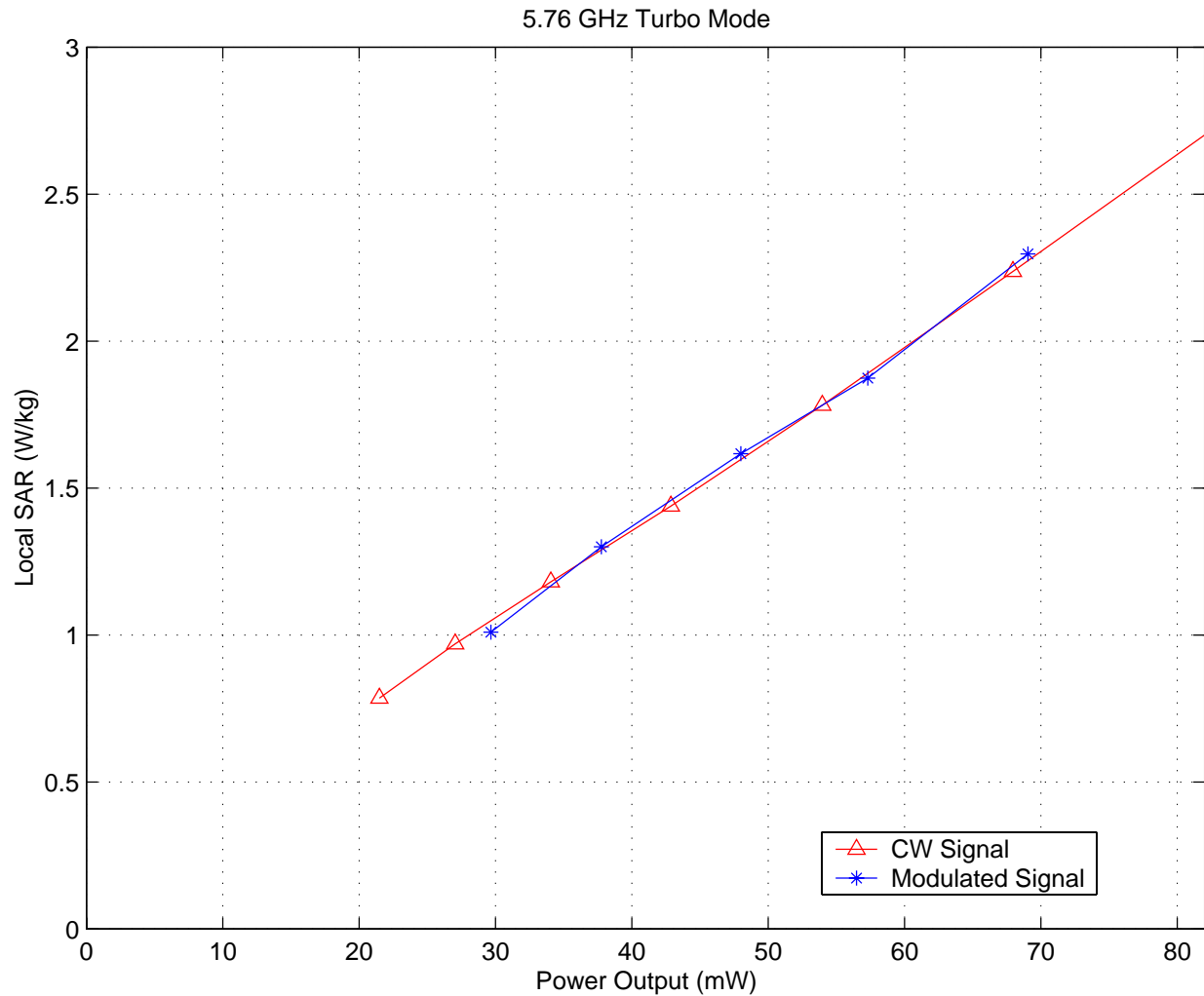


Fig. A.4. Comparison of the SAR for CW or OFDM modulated signals for the turbo mode at 5.76 GHz.

APPENDIX B  
**SAR System Validation for the 802.11a Band**

The measured SAR distribution for the peak 1-g SAR region using WR187 rectangular waveguide radiation system.

**For December 5, 2003 – The SAR plot at 5.25 GHz**

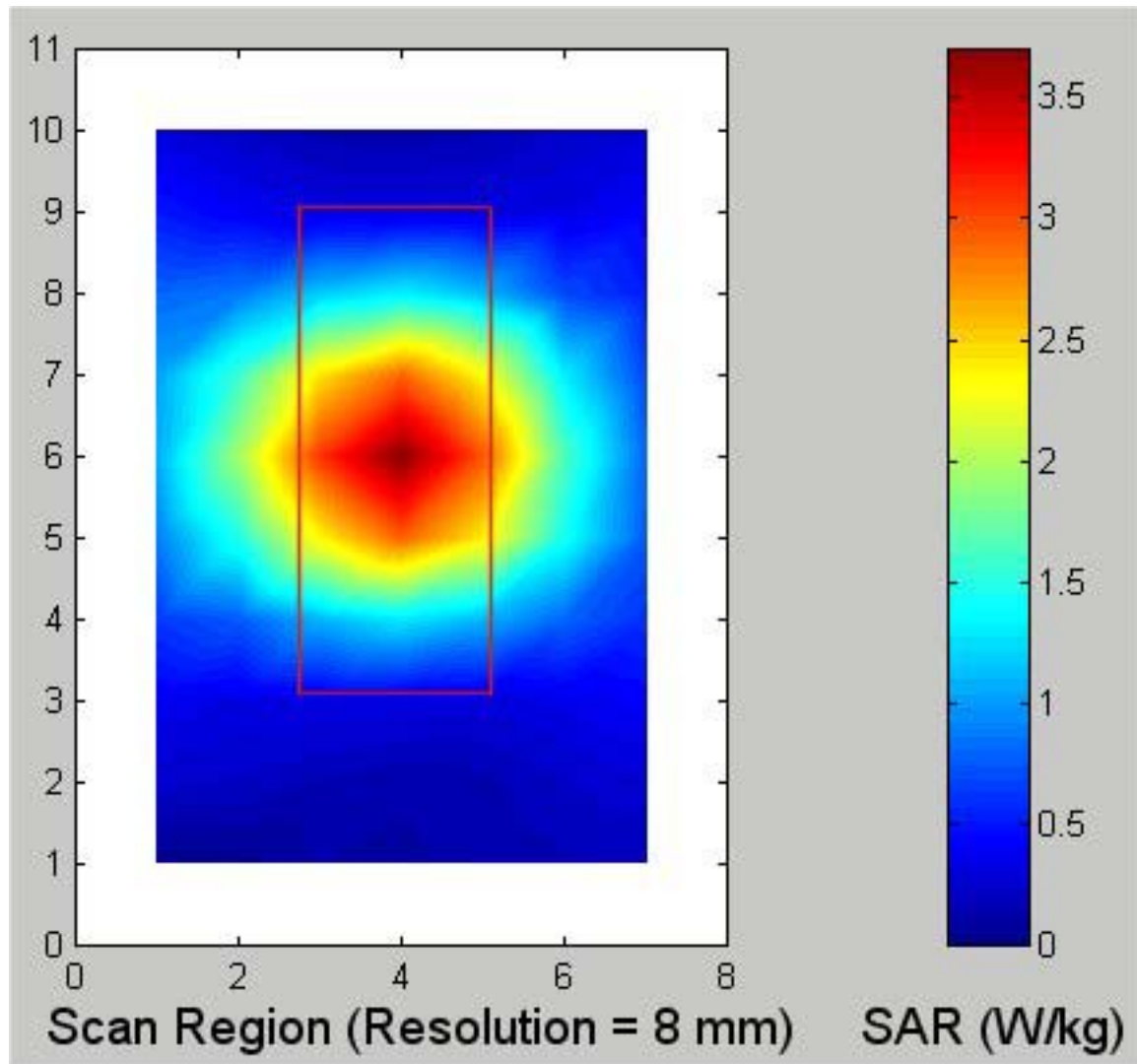


Fig. B.1. Coarse scans of the measured SAR distribution for the WR187 rectangular waveguide irradiation system for system verification at 5.25 GHz. Also shown is the outline of the rectangular waveguide overlaid on the SAR contours. Radiated power = 100 mW.

**December 5, 2003**

**1-g SAR = 3.610 W/kg**

**a. At depth of 1 mm**

8.782	9.587	9.709	9.092	8.480
9.448	9.946	10.299	10.138	9.248
9.741	10.284	10.378	10.276	9.358
9.192	9.822	10.023	9.761	9.146
8.582	8.954	9.463	9.292	8.559

**b. At depth of 3 mm**

4.314	4.692	4.770	4.545	4.269
4.608	4.928	5.076	4.936	4.579
4.680	5.009	5.130	5.008	4.640
4.484	4.833	4.973	4.798	4.495
4.165	4.458	4.623	4.507	4.197

**c. At depth of 5 mm**

2.042	2.206	2.260	2.188	2.066
2.155	2.329	2.394	2.307	2.168
2.153	2.324	2.419	2.338	2.200
2.091	2.279	2.358	2.255	2.107
1.919	2.114	2.160	2.093	1.971

**d. At depth of 7 mm**

1.023	1.098	1.133	1.093	1.031
1.064	1.137	1.175	1.135	1.060
1.051	1.125	1.178	1.144	1.082
1.023	1.122	1.155	1.106	1.026
0.921	1.029	1.059	1.027	0.973

**e. At depth of 9 mm**

0.589	0.636	0.648	0.607	0.567
0.609	0.628	0.652	0.637	0.578
0.597	0.624	0.649	0.638	0.599
0.579	0.628	0.636	0.620	0.570
0.512	0.562	0.597	0.585	0.555

For December 5, 2003 – The SAR plot at 5.80 GHz

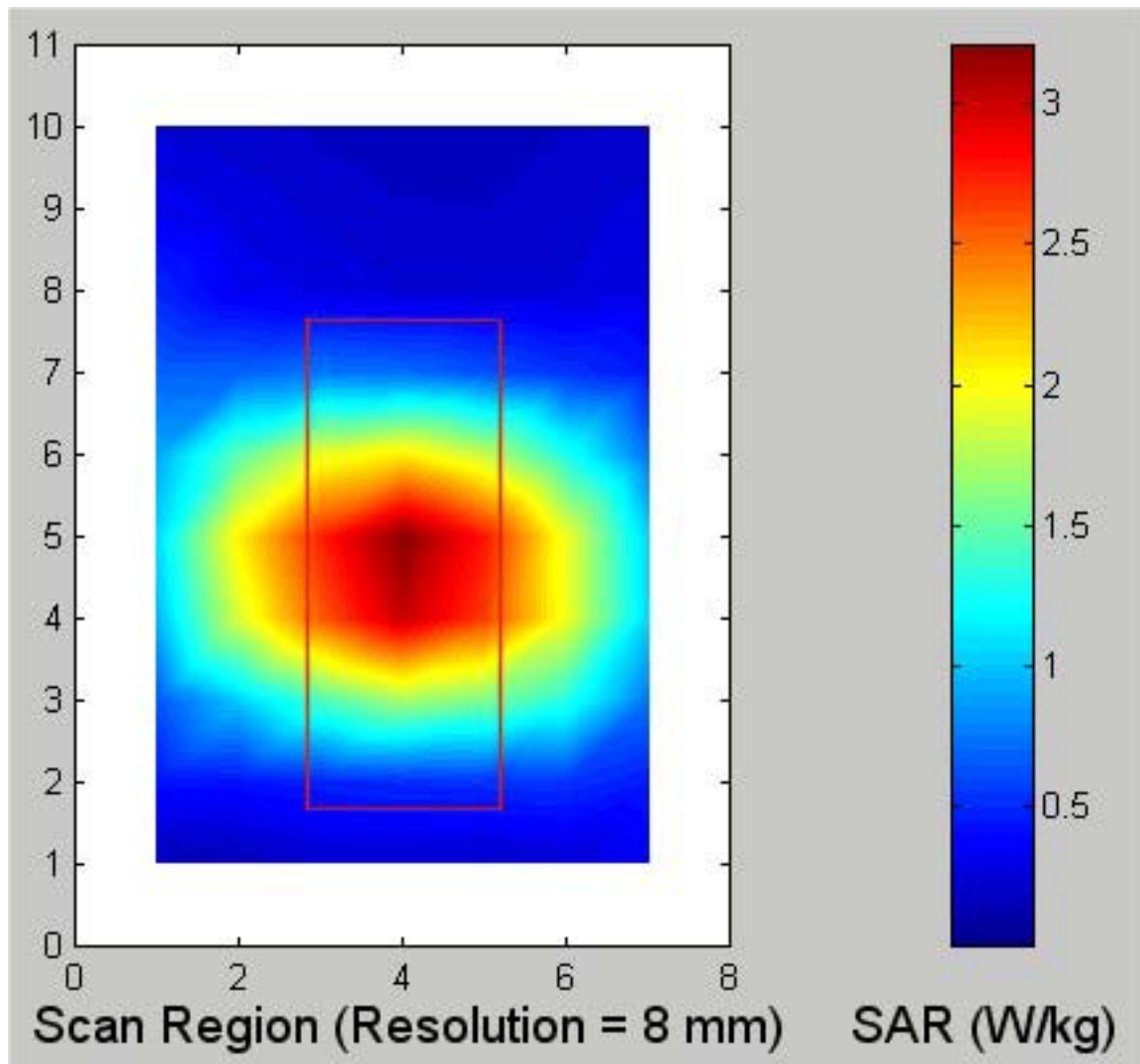


Fig. B.2. Coarse scans of the measured SAR distribution for the WR187 rectangular waveguide irradiation system for system verification at 5.80 GHz. Also shown is the outline of the rectangular waveguide overlaid on the SAR contours. Radiated power = 100 mW.

**December 5, 2003**

**1-g SAR = 3.930 W/kg**

**a. At depth of 1 mm**

10.541	11.182	11.029	11.013	10.418
11.319	11.581	11.708	11.683	10.822
11.603	11.895	11.838	11.800	10.989
11.644	11.846	11.653	11.655	11.233
11.265	11.243	11.569	11.287	10.982

**b. At depth of 3 mm**

4.630	4.825	4.797	4.776	4.603
4.904	5.050	5.106	5.018	4.750
5.005	5.155	5.179	5.096	4.862
5.020	5.128	5.127	5.055	4.877
4.859	4.919	4.997	4.902	4.738

**c. At depth of 5 mm**

1.885	1.904	1.920	1.908	1.871
1.948	2.013	2.045	1.970	1.926
1.970	2.034	2.063	2.020	1.974
1.981	2.035	2.065	2.001	1.940
1.913	1.975	1.979	1.956	1.881

**d. At depth of 7 mm**

0.857	0.839	0.857	0.850	0.829
0.857	0.879	0.898	0.861	0.860
0.857	0.877	0.886	0.886	0.868
0.874	0.888	0.898	0.867	0.852
0.833	0.869	0.870	0.866	0.839

**e. At depth of 9 mm**

0.541	0.530	0.538	0.528	0.501
0.528	0.540	0.539	0.532	0.523
0.530	0.535	0.529	0.535	0.523
0.553	0.531	0.535	0.526	0.524
0.516	0.527	0.534	0.538	0.528

## APPENDIX C

## SCREEN DUMPS FOR THE UNIVERSITY OF UTAH TISSUE-SIMULANT FLUID FOR THE FREQUENCY BAND 5.0 TO 6.0 GHz (FIVE REPEATED MEASUREMENTS)

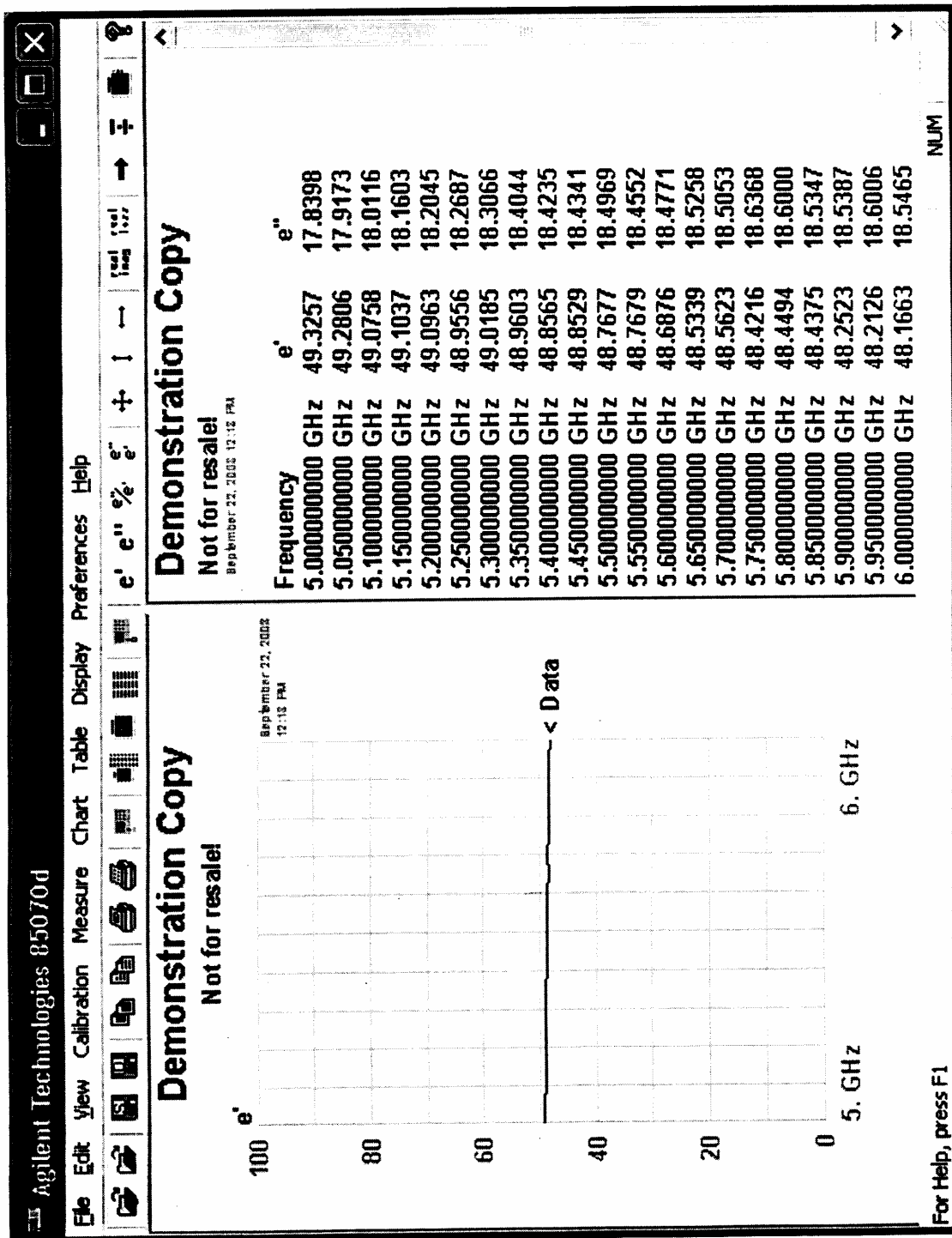


Fig. C.1.

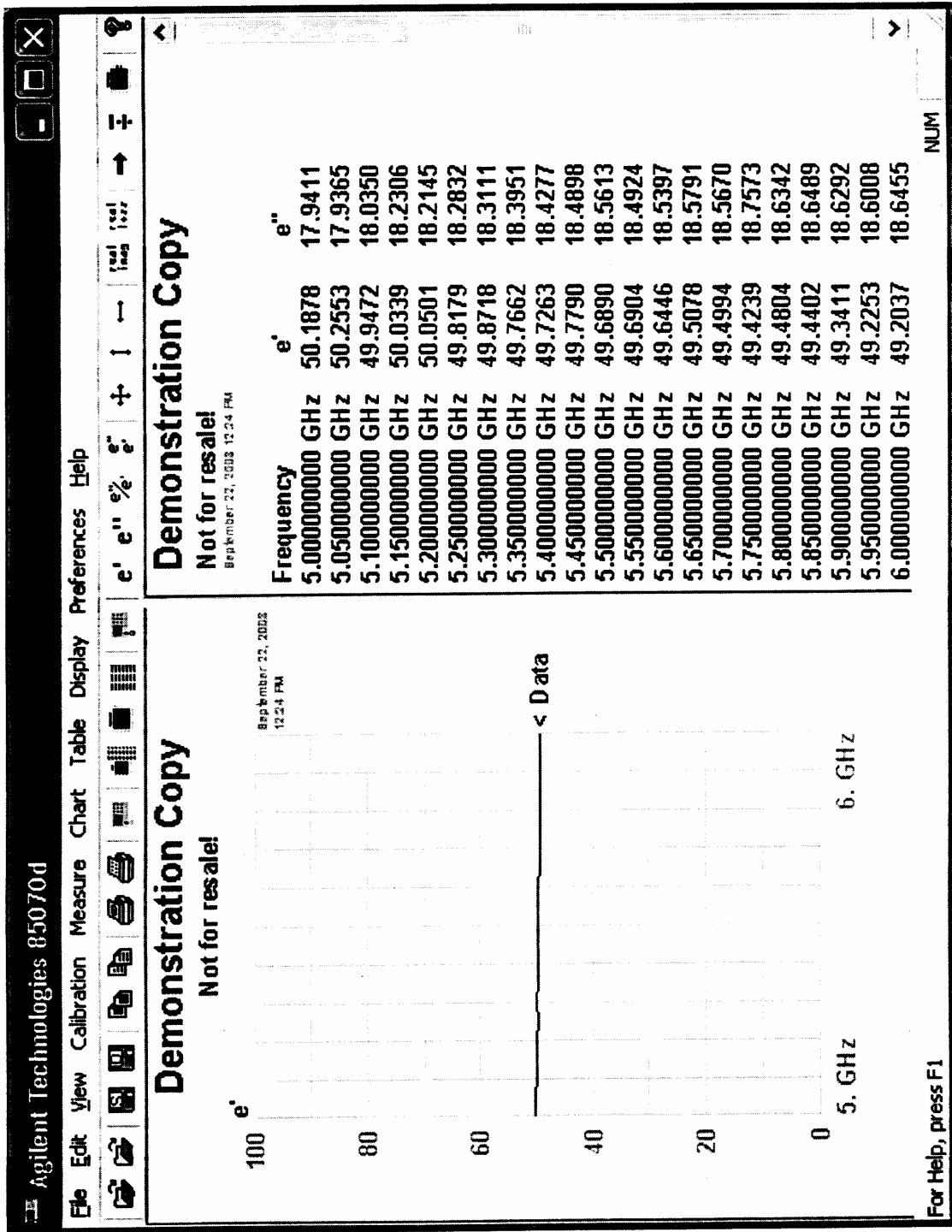


Fig. C.2.

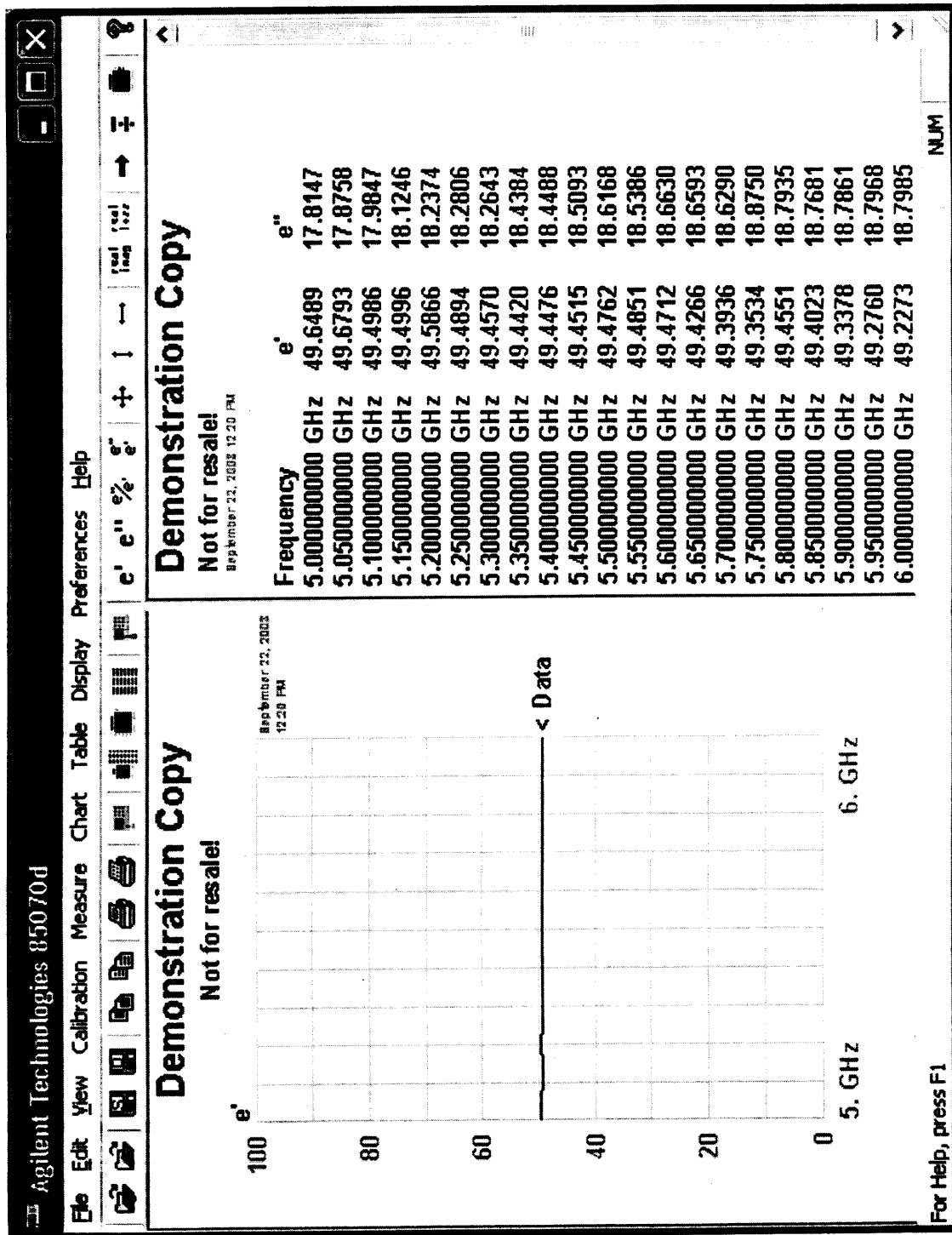


Fig. C.3

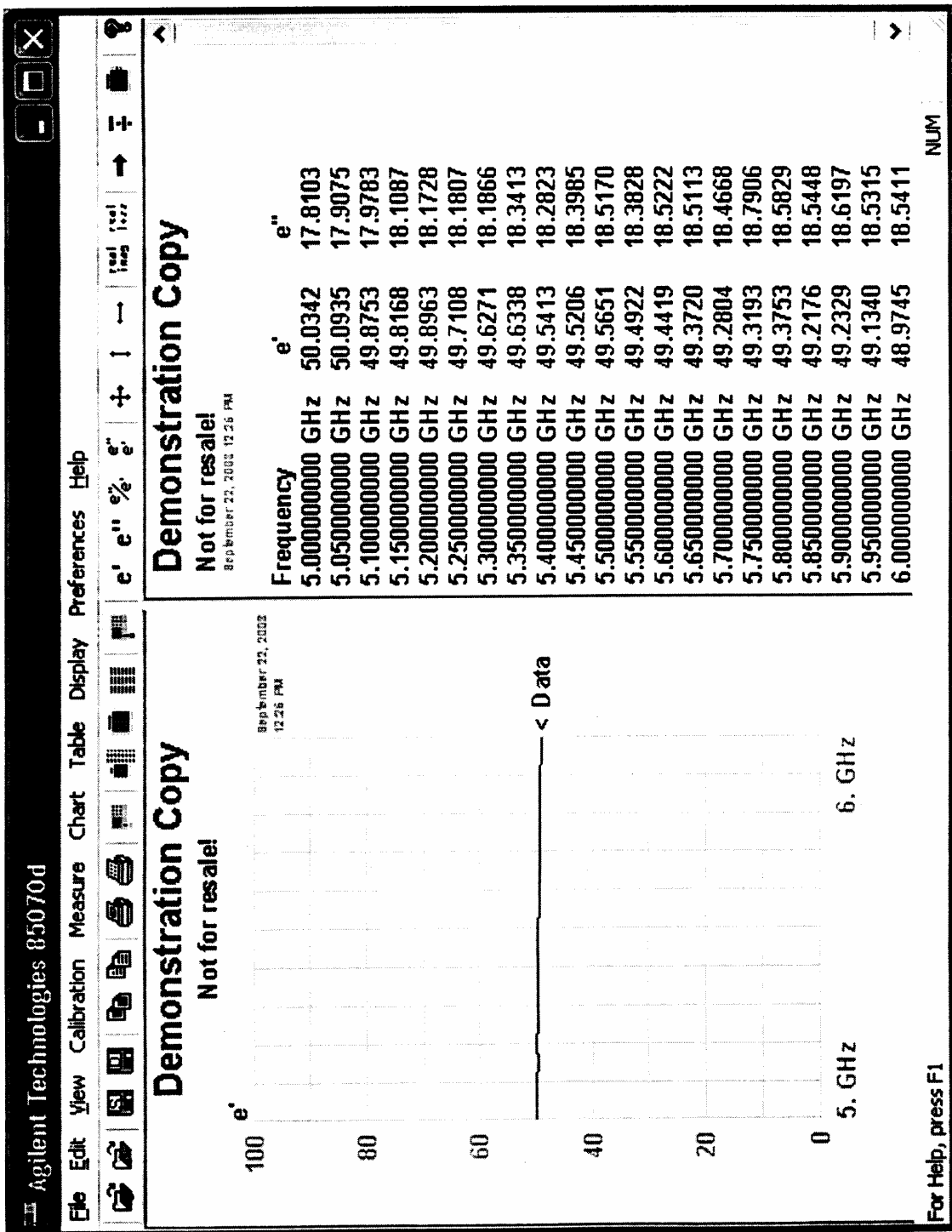


Fig. C.4.

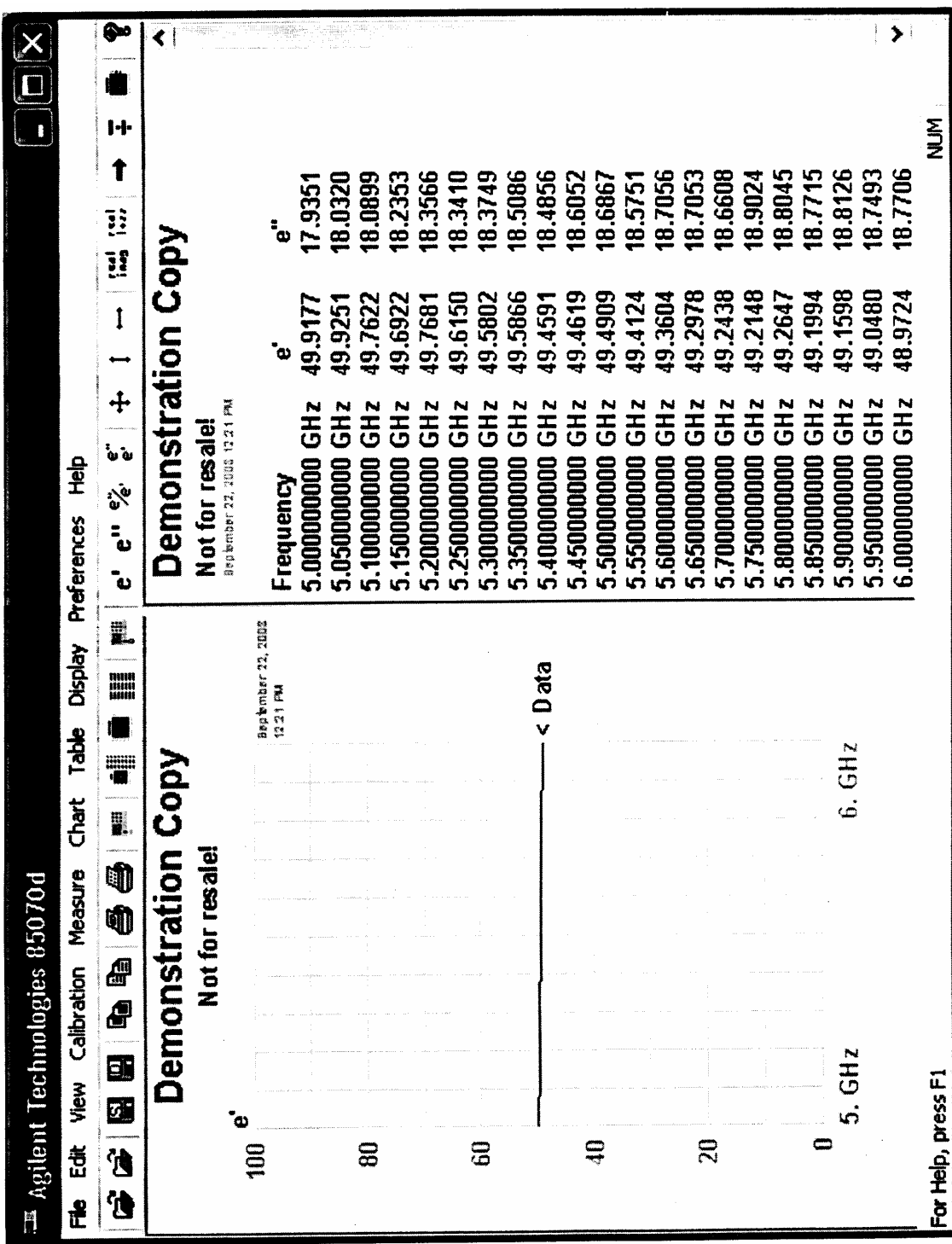


Fig. C.5.

## APPENDIX D

### AN OPEN-ENDED WAVEGUIDE SYSTEM FOR SAR SYSTEM VALIDATION AND/OR PROBE CALIBRATION FOR FREQUENCIES ABOVE 3 GHz

Qingxiang Li, Student Member, IEEE

Om P. Gandhi, Life Fellow, IEEE, and

Gang Kang, Senior Member, IEEE

Department of Electrical and Computer Engineering

University of Utah

Salt Lake City, Utah 84112, U.S.A.

#### Abstract

Compliance with safety guidelines prescribed in terms of maximum electromagnetic power absorption (specific absorption rate or SAR) for any 1- or 10-g of tissue is required for all newly-introduced personal wireless devices such as Wi-Fi PCs. The prescribed SAR measuring system is a planar phantom with a relatively thin base of thickness 2.0 mm filled with a lossy fluid to simulate dielectric properties of the tissues. A well-characterized, broadband irradiator is required for SAR system validation and/or submerged E-field probe calibration for the new 802.11a frequencies in the 5-6 GHz band. We describe an open-ended waveguide system that may be used for this purpose. Using a fourth-order polynomial least-square fit to the experimental data gives SAR variations close to the bottom surface of the phantom that are in excellent agreement with those obtained using the FDTD numerical method. The experimentally-determined peak 1-g SARs are within 1 to 2 percent of those obtained using the FDTD both at 5.25 and 5.8 GHz.

Index Terms – Broadband, electromagnetic exposure system, probe calibration, safety assessment, comparison with numerical calculations

Submitted to *IEEE Transactions on Microwave Theory and Techniques*, June 10, 2003.

# AN OPEN-ENDED WAVEGUIDE SYSTEM FOR SAR SYSTEM VALIDATION AND/OR PROBE CALIBRATION FOR FREQUENCIES ABOVE 3 GHz

Qingxiang Li, Student Member, IEEE  
Om P. Gandhi, Life Fellow, IEEE, and  
Gang Kang, Senior Member, IEEE

## I. Introduction

Compliance with the safety guidelines such as those proposed by IEEE [1] ICNIRP [2], etc. is required by regulatory agencies in the United States and elsewhere for all newly-introduced personal wireless devices such as Wi-Fi PCs, cellular telephones, etc. These safety guidelines are set in terms of maximum 1- or 10-g mass-normalized rates of electromagnetic energy deposition (specific absorption rates or SARs) for any 1- or 10-g of tissue. The two most commonly-used SAR limits today are those of IEEE [1] – 1.6 W/kg for any 1 g of tissue, and ICNIRP [2] – 2 W/kg for any 10 g of tissue, excluding extremities such as hands, wrists, feet, and ankles where higher SARs up to 4 W/kg for any 10 g of tissue are permitted in both of these standards. Experimental and numerical techniques using planar or head-shaped phantoms have been proposed for determining compliance with the SAR limits [3-5]. For frequencies above 800 MHz, the size of a rectangular waveguide is quite manageable and use of an appropriate waveguide filled with a tissue-simulant medium is recommended for calibration of an E-field probe in FCC Supplement C, Edition 01-01 to OET Bulletin 65 [6]. Even though no recommendation is made on choice of an irradiation system for frequencies above 3 GHz, balanced half-wave dipoles have been suggested for system validation for frequencies less than or equal to 3 GHz [6]. It is very difficult to develop half-wave dipole antennas for use in the 5.1 to 5.8 GHz band both because of fairly small dimensions and the resulting dimensional tolerances, and relatively narrow bandwidths of the required baluns – balanced to unbalanced transformers (typically less than 10-12% for  $VSWR < 2.0$  and less than 5-6% for  $VSWR < 1.5$ ). On the other hand, rectangular waveguides are broadband with simultaneous bandwidths larger than 1-2 GHz and are fairly easy to use for frequencies in excess of 3 GHz. We have, therefore, developed an open-ended waveguide system for SAR system validation and/or probe calibration in the frequency band 5 to 6 GHz. This is a band that is presently being used for 802.11a antennas of Wi-Fi PCs.

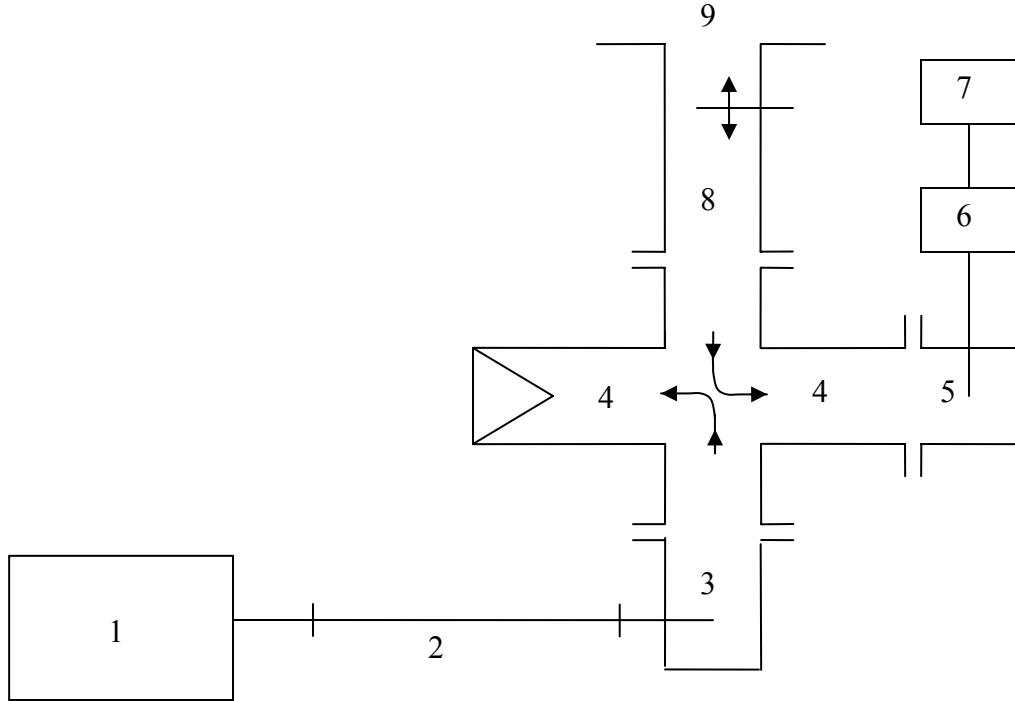
## II. The Waveguide Irradiation System

For the 5-6 GHz band, we have used a WR187 rectangular waveguide of internal dimensions  $4.75 \times 2.21$  cm. The operating ( $TE_{10}$  mode) band of this waveguide is from 3.95 to 5.85 GHz. This is considerably larger than the required overall bandwidth of 675 MHz for the IEEE 802.11a frequency bands of 5.15-5.35 and 5.745 to 5.825 GHz. The waveguide irradiation system used for SAR system validation is shown in Fig. 1. As recommended in [6], the open-ended waveguide irradiator is placed at a distance of 8 mm below the base of planar phantom with inside dimensions of  $30.5 \times 41.9$  cm and a base thickness of  $2.0 \pm 0.2$  mm. This results in the open end of the waveguide at a distance of 10 mm below the lossy tissue-simulant fluid in the phantom. The microwave circuit arrangement used for the waveguide irradiation system is shown in Fig. 2. As shown in Fig. 2, the WR187 waveguide is fed with microwave power from a

Hewlett Packard Model 83620A Synthesized Sweeper (10 MHz-20 GHz). When placed at a distance of 8 mm below the base of the planar phantom, the reflection coefficient is about 10-20%. Even this relatively small amount of reflection has been greatly reduced to less than 0.5% by using a movable slide-screw waveguide tuner (Narda Model 22CI). The planar phantom is filled to a depth of 15 cm with a fluid to simulate dielectric properties recommended for the body phantom in [6]. The dielectric constants  $\epsilon_r$  and conductivities  $\sigma$  at the experimental frequencies of 5.25 and 5.8 GHz are similar to those recommended in the SAR Compliance Standards used in the U.S. and in Europe [3, 4]. For our experiments and calculations,  $\epsilon_r = 48.8$ ,  $\sigma = 6.82$  S/m at 5.25 GHz; and  $\epsilon_r = 46.9$ ,  $\sigma = 7.83$  S/m at 5.8 GHz.



Fig. 1. Photograph of the rectangular waveguide radiator used for system validation. Also seen is the Narda Model 22CI movable slide screw tuner used to match the input power at 5.25 or 5.8 GHz to the planar tissue-simulant phantom.



1. Hewlett Packard (HP) Model 83620A Synthesized Sweeper (10 MHz-20 GHz).
2. Coaxial line.
3. Coaxial to waveguide adapter.
4. 20 dB crossguide coupler (may be reversed to measure incident power).
5. HP Model G281A coaxial to waveguide adapter
6. HP Model 8482A power sensor.
7. HP Model 436A power meter.
8. Narda Microline® Slide Screw Tuner Model 22CI.
9. Radiating open end of the waveguide.

Fig. 2. The microwave circuit arrangement used for SAR system validation.

### III. Calculation of the SAR Distributions

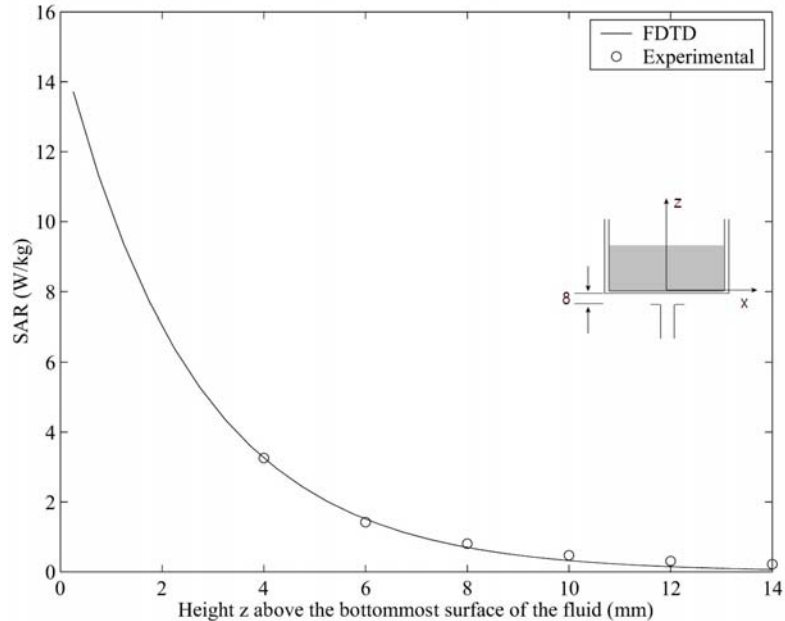
We have used the well-established finite-difference time-domain (FDTD) numerical electromagnetic method to calculate the electric fields and SAR distributions for the planar phantom of base thickness 2.0 mm of dielectric constant  $\epsilon_r = 2.56$  and dielectric properties of the tissue-simulant lossy fluid as given in Section II. The FDTD method described in several texts [7, 8] has been successfully used by various researchers [9-12] and, therefore, would not be described here. For the FDTD calculations, we have used a cell size  $\delta = 0.5$  mm in order to meet the requirement  $\delta \leq \lambda_e / 10$  in the lossy fluid. The calculated variations of the SAR distribution at the experimental frequencies of 5.25 and 5.80 GHz are given in Figs. 3 a-c and 4

a-c, respectively. Also shown in the same figures are the experimental values of the SARs (shown by circles). From Figs. 3 and 4, it is obvious that the penetration of electromagnetic fields in the 5.1 to 5.8 GHz band is extremely shallow. The calculated depths of penetration corresponding to  $1/e^2$ -reduction of SAR (13.5% of the SAR at the surface) are only 6.85 and 5.985 mm at 5.25 and 5.8 GHz, respectively. Both of these depths of penetration are very similar to those obtained for plane-wave irradiation at these frequencies (7.15 mm for 5.25 GHz and 6.25 mm for 5.8 GHz).

## IV. Experimental Setup and Measurements

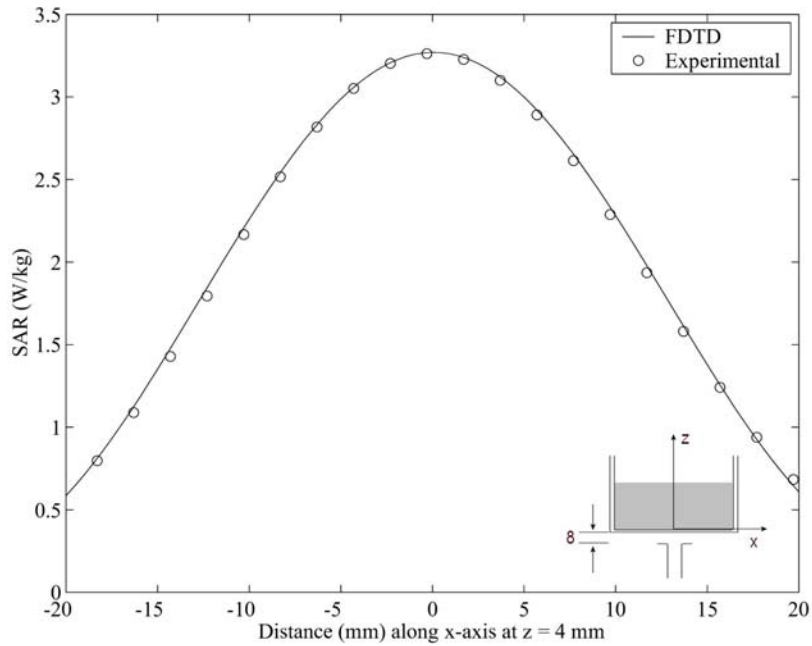
### A. Experimental Setup

As recommended in FCC Bulletin 65 [14], a planar phantom of fairly thin base thickness 2.0 mm of relatively low dielectric constant ( $\epsilon_r = 2.56$  in our case) is used for the determination of SAR distributions of wireless PCs and for the SAR system validation. The lateral dimensions of the planar phantom (in our case  $30.5 \times 41.9$  cm) are large enough to ignore scattering from the edges of the rectangular box or the tissue-simulant lossy fluid used to fill this box to a depth of 10-15 cm (several times the depth of penetration of fields in the fluid so as to present a nearly infinitely deep medium to neglect reflections). A photograph of the phantom model together with a computer-controlled 3-D stepper motor system (Arrick Robotics MD-2A) is shown in Fig. 5.

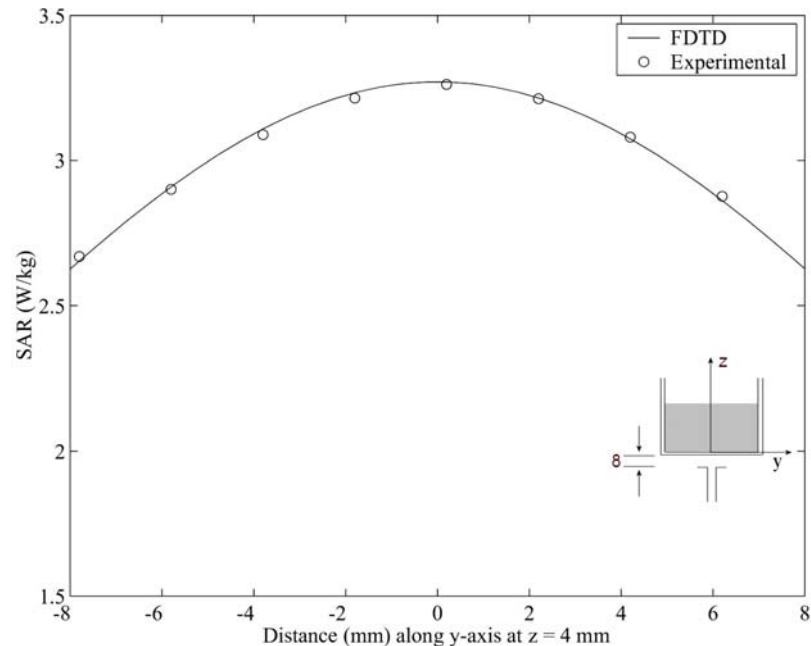


a. Variation of SAR along the z-axis.

Fig. 3. Comparison of the measured and calculated SAR variations for a planar phantom of base thickness 2.0 mm and internal dimensions  $30.5 \times 41.9 \times 20$  cm for a WR 187 open-ended waveguide radiator placed 10 mm below the bottommost surface of the lossy tissue-simulant phantom. Frequency = 5.25 GHz.

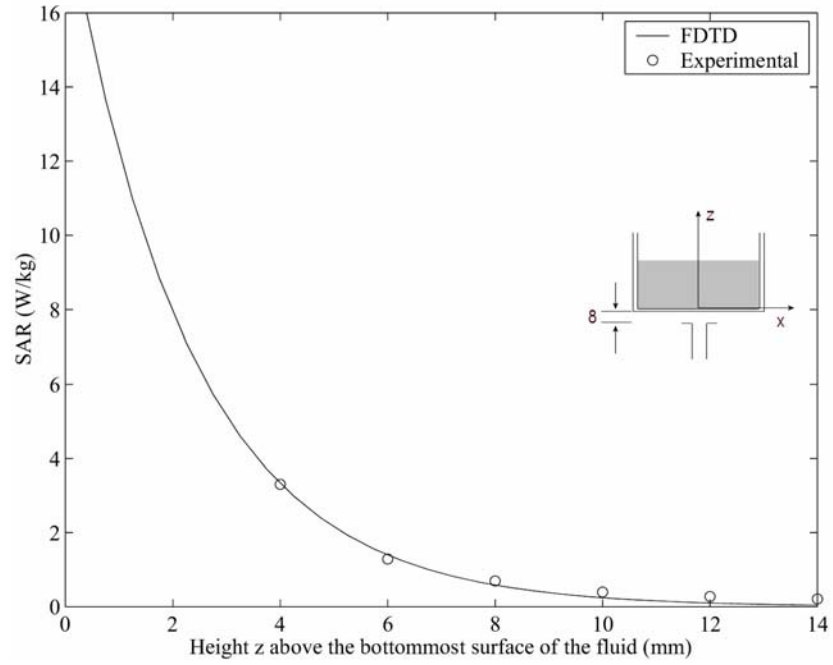


b. Variation of SAR along the x-axis parallel to the broader dimension of the waveguide at height  $z = 4$  mm.

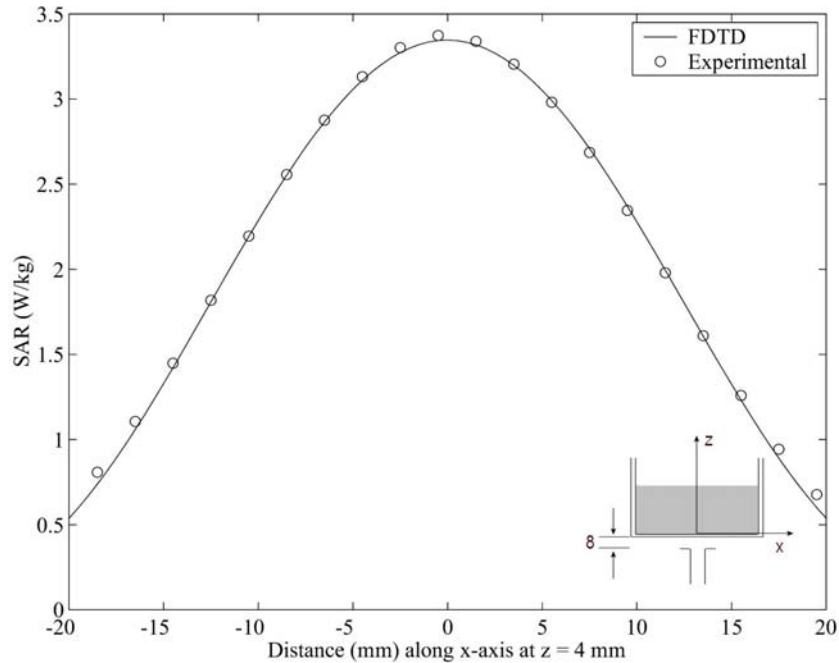


c. Variation of SAR along the y-axis parallel to the narrower dimension of the waveguide at height  $z = 4$  mm.

Fig. 3. Comparison of the measured and calculated SAR variations for a planar phantom of base thickness 2.0 mm and internal dimensions  $30.5 \times 41.9 \times 20$  cm for a WR 187 open-ended waveguide radiator placed 10 mm below the bottommost surface of the lossy tissue-simulant phantom. Frequency = 5.25 GHz.

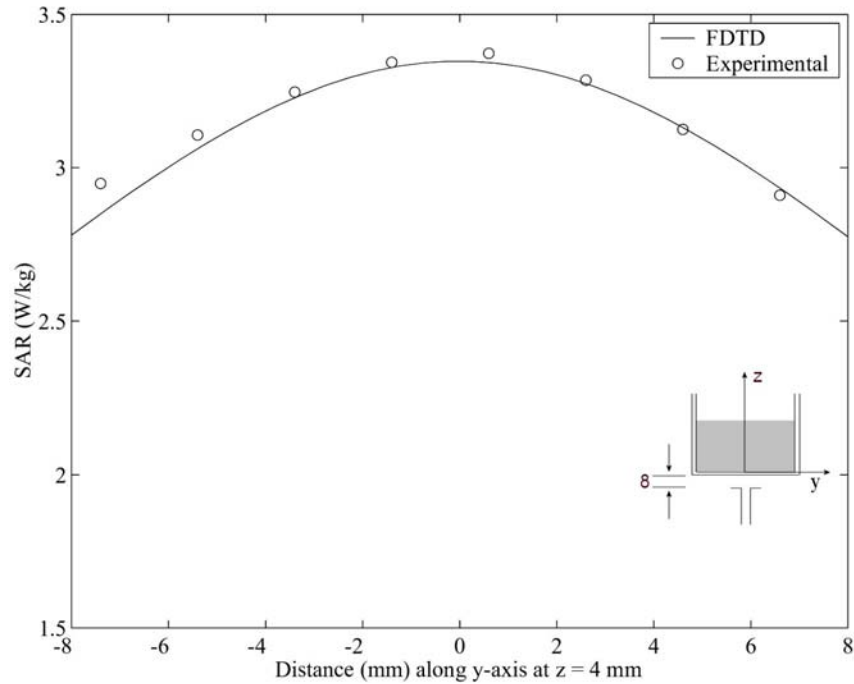


a. Variation of SAR along the z-axis.



b. Variation of SAR along the x-axis parallel to the broader dimension of the waveguide at height  $z = 4$  mm.

Fig. 4. Comparison of the measured and calculated SAR variations for a planar phantom of base thickness 2.0 mm and internal dimensions  $30.5 \times 41.9 \times 20$  cm for a WR 187 open-ended waveguide radiator placed 10 mm below the bottommost surface of the lossy tissue-simulant phantom. Frequency = 5.8 GHz.



c. Variation of SAR along the y-axis parallel to the narrower dimension of the waveguide at height  $z = 4$  mm.

Fig. 4. Comparison of the measured and calculated SAR variations for a planar phantom of base thickness 2.0 mm and internal dimensions  $30.5 \times 41.9 \times 20$  cm for a WR 187 open-ended waveguide radiator placed 10 mm below the bottommost surface of the lossy tissue-simulant phantom. Frequency = 5.8 GHz.

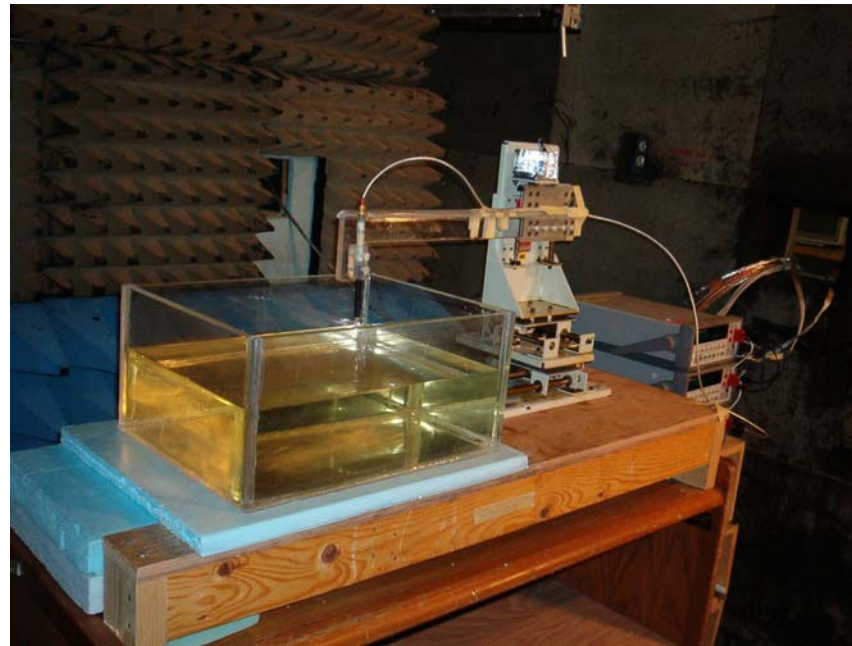


Fig. 5. Photograph of the planar model with the 3-D stepper motor system used for measurement of SAR variation for comparison with FDTD calculations.

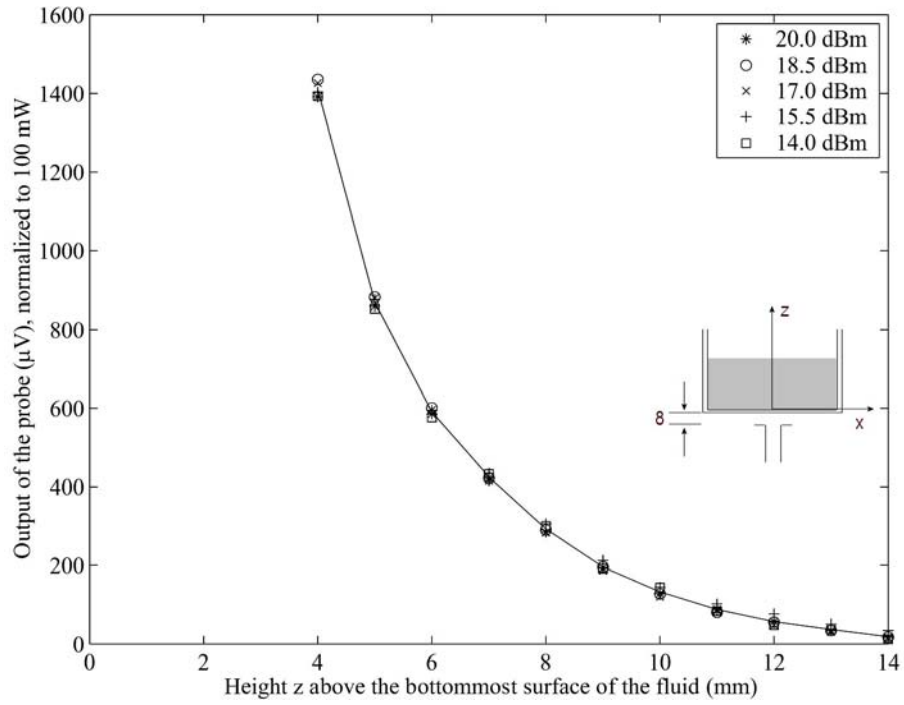
A triaxial Narda Model 8021 E-field probe is used to determine the internal electric fields. The positioning repeatability of the stepper motor system moving the E-field probe is within  $\pm 0.1$  mm. Outputs from the three channels of the E-field probe are dc voltages, the sum of which is proportional to the square of the internal electric fields ( $|E_i|^2$ ) from which the SAR can be obtained from the equation:  $SAR = \sigma(|E_i|^2)/\rho$ , where  $\sigma$  and  $\rho$  are the conductivity and mass density of the tissue-simulant material, respectively [13]. The dc voltages for the three channels of the E-field probe are read by three HP 34401A multimeters and sent to the computer via an HPIB interface. The setup is carefully grounded and shielded to reduce the noise due to the electromagnetic interference (EMI).

### ***B. E-Field Probe***

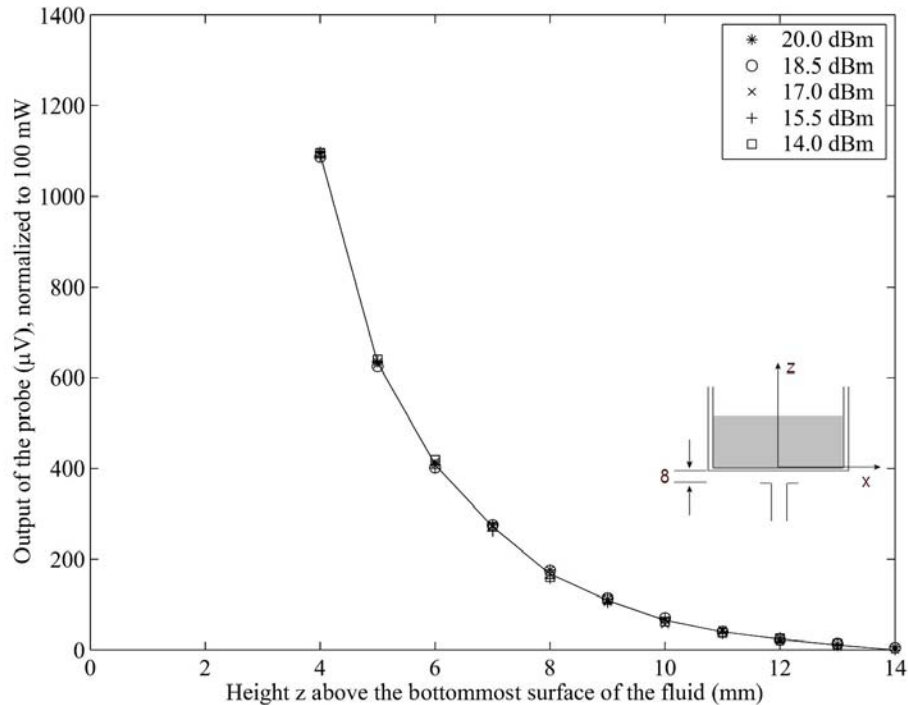
The nonperturbing implantable E-field probe used in the setup was originally developed by Bassen et al. [14] and is manufactured by L3/Narda Microwave Corporation, Hauppauge, NY as Model 8021 E-field probe. In the probe, three orthogonal miniature dipoles each of length approximately 2.5 mm are placed on a triangular-beam substrate. Each dipole is loaded with a small Schottky diode and connected to the external circuitry by high resistance ( $2 M\Omega \pm 40\%$ ) leads to reduce secondary pickups. The entire structure is then encapsulated with a low dielectric constant insulating material. The probe thus constructed has a very small diameter (4 mm), which results in a relatively small perturbation of the internal electric field. The probe is rated for frequencies up to 3 GHz for tissue-simulant media, but is presently used for system validation at frequencies in the 5 to 6 GHz range. Consequently, the probe had to be checked for square-law performance, and isotropy for use at these higher frequencies.

1. **Test for Square-Law Region:** It is necessary to operate the E-field probe in the square-law region for each of the diodes so that the sum of the dc voltage outputs from the three dipoles is proportional to the square of the internal electric field ( $|E_i|^2$ ). Fortunately, the personal wireless devices such as the PCs induce SARs that are generally less than 5-6 W/kg even for closest locations to the body. For SAR measurements, it is, therefore, necessary that the E-field probe be checked for square-law behavior for SARs up to such values that are likely to be encountered. Such a test may be conducted using a canonical lossy body such as a rectangular box used here. By varying the radiated power of the waveguide, the output of the probe should increase linearly with the applied power for each of the test locations.

Shown in Fig. 6a and b are the results of the tests performed to check the square-law behavior of the E-field probe used in our setup at 5.25 and 5.8 GHz, respectively. Used as the radiator is the WR 187 waveguide placed at a distance of 8 mm below the base of the planar phantom (10 mm below the bottom surface of the tissue-simulant fluid as recommended in [6]).



a. Test for square-law behavior at 5.25 GHz.



b. Test for square-law behavior at 5.8 GHz.

Fig. 6. Variation of the output voltage (proportional to  $|E_i|^2$ ) for different radiated powers normalized to 100 mW (20 dBm).

Since the dc voltage outputs of the probe are fairly similar when normalized to a radiated power of 100 mW, the square-law behavior is demonstrated and an output voltage that is proportional to  $|E_i|^2$  is obtained within  $\pm 2.2\%$  both at 5.25 and 5.8 GHz.

2. **Test for Isotropy of the Probe:** Another important characteristic of the probe that affects the measurement accuracy is its isotropy. Since the orientation of the induced electric field is generally unknown, the E-field probe should be relatively isotropic in its response to the orientation of the E-field. Shown in Fig. 7a and b are the test results of the E-field probe used in our setup at 5.25 and 5.8 GHz, respectively. The E-field probe was rotated around its axis from 0-180° in incremental steps of 15°. Because of the alternating nature of the fields, angles of  $\theta$  and  $180^\circ + \theta$  are identical, hence 0-165° rotation of the E-field probe was considered to be adequate to cover the entire 360° rotation of the probe. As seen in Fig. 7a and b, an isotropy of less than  $\pm 0.18$  dB ( $\pm 4.3\%$ ) was observed for this E-field probe both at 5.25 and 5.8 GHz.
3. **Calibration of the E-Field Probe:** Since the voltage output of the E-field probe is proportional to the square of the internal electric field ( $|E_i|^2$ ), the SAR is, therefore, proportional to the voltage output of the E-field probe by a proportionality constant C. The constant C is defined as the calibration factor and is frequency and material dependent. It is measured to calibrate the probe at the various frequencies of interest using the appropriate tissue-simulating materials for the respective frequencies.

Canonical geometries such as waveguides, rectangular slabs, and layered or homogeneous spheres have, in the past, been used for the calibration of the implantable E-field probe [15-17] albeit at lower frequencies. Since the FDTD method has been carefully validated to solve electromagnetic problems for a variety of near-field exposure geometries [18], we were able to calibrate the Narda E-field probe by comparing the measured variations of the probe voltage (proportional to  $|E_i|^2$ ) against the FDTD-calculated variations of the SARs for the planar phantom of base thickness 2.0 mm ( $\epsilon_r = 2.56$ ) and internal dimensions  $30.5 \times 41.9 \times 20$  cm irradiated by the WR 187 waveguide placed below this phantom as previously described in Section. II. Shown in Figs. 6a, b and 7a, b are the comparisons between the experimentally measured and FDTD-calculated variations of the SAR distributions in the tissue-simulant fluid. Since there are excellent agreements between the calculated SARs and the measured variations of the voltage outputs of the E-field probe, it is possible to calculate the calibration factors at the respective frequencies by fitting the measured data to the FDTD-calculated results by means of the least mean-square error (LMSE) method. For the Narda Model 8021 E-field probe used in our setup, the calibration factor is determined to be 2.98 (mW/kg)/ $\mu$ V  $\pm 5\%$  both at 5.25 and 5.8 GHz, respectively.

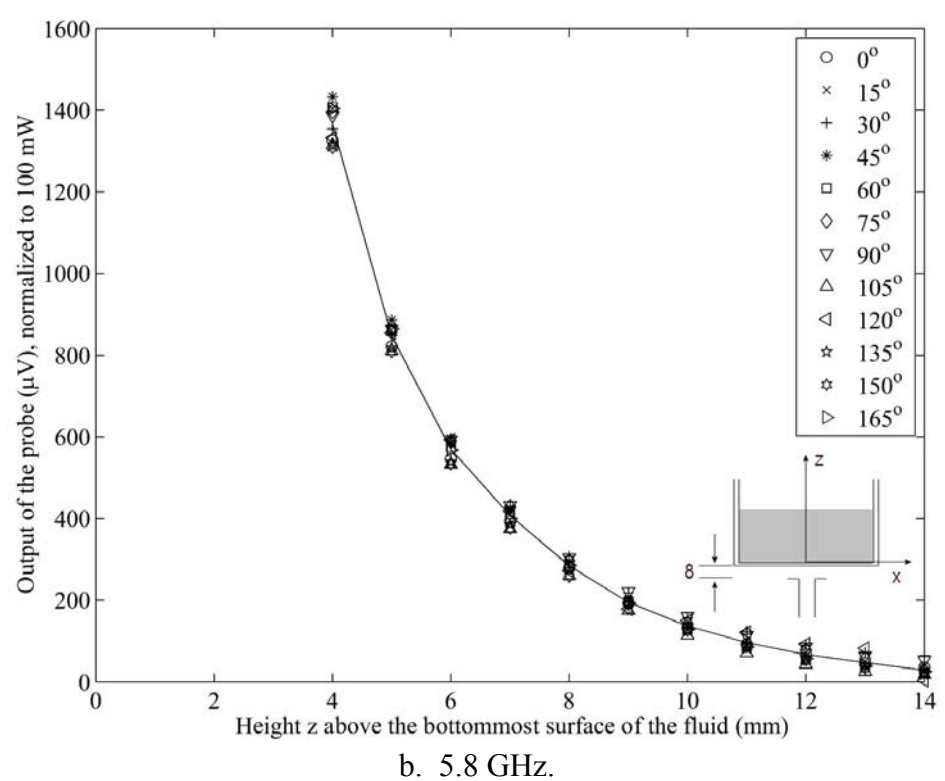
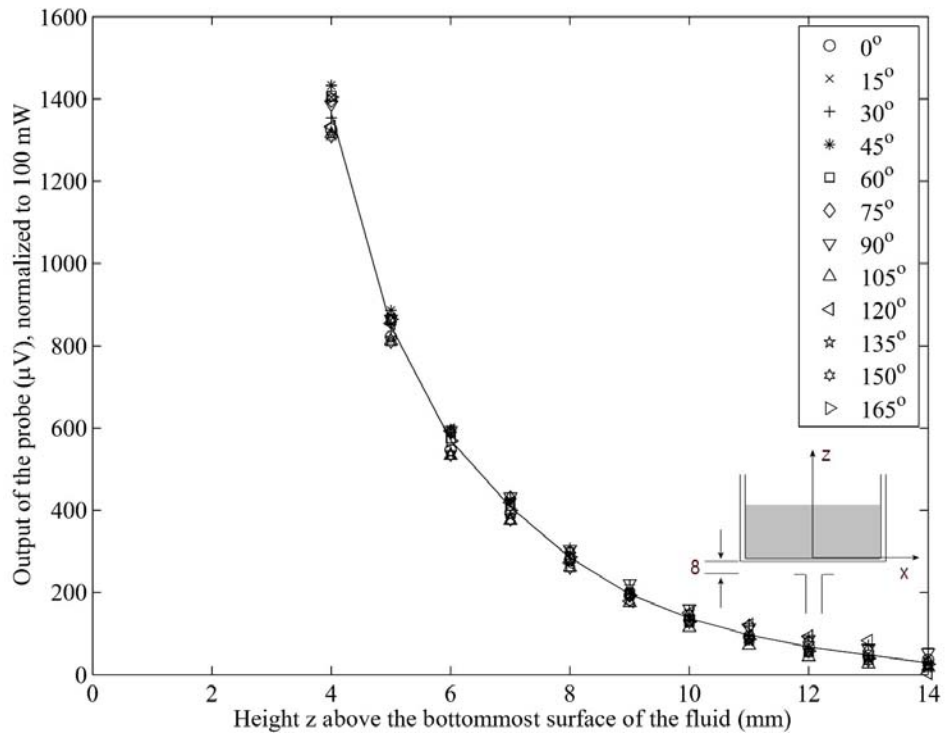


Fig. 7. Test for isotropy.

#### IV. Need for Extrapolation

Because of the physical separation of the three orthogonal pickup dipoles from the tip of the E-field probe, the SAR measurements cannot be taken any closer than about 3 mm from the bottom surface of the phantom fluid. As given in Figs. 8 and 9, we have measured the SARs with 2 mm resolution at heights of 4, 6, 8, 10, 12 and 14 mm above the bottom surface of the phantom fluid. We have tried second-, third-, fourth-, and fifth-order polynomial least-square fits to extrapolate the measured data to obtain SARs closer to the bottom of the lossy fluid. As seen in Figs. 8 and 9, the second- and third-order polynomials underestimate the SARs while the fifth-order polynomial overestimates the SAR distribution. An excellent least-square fit to the numerically-calculated SAR variations is obtained by using a fourth-order polynomial to extrapolate the measured data both at 5.25 and 5.8 GHz.

After identifying the region of the highest SAR, the SAR distributions were measured with a finer resolution of 2 mm in order to obtain the peak  $1\text{ cm}^3$  or 1-g SAR. Here too, the SAR measurements were performed for the xy planes at heights  $z$  of 4, 6, 8, 10, 12, and 14 mm from the bottom surface of the body-simulant fluid. The SARs thus measured were extrapolated using a fourth-order least-square fit to the measured data to obtain values at 1, 3, 5, 7, and 9 mm height and used to obtain peak 1-g SARs. For a radiated power of 100 mW, the SARs thus obtained with 2 mm resolution for xy planes at heights  $z$  of 1, 3, 5, 7, and 9 mm for the peak SAR region of volume  $10 \times 10 \times 10$  mm were used to obtain peak 1-g SAR at 5.25 and 5.8 GHz, respectively. The experimentally-determined peak 1-g SARs for 100 mW of radiated power of 3.678 and 3.947 W/kg are extremely close to the FDTD-calculated 1-g SARs for this waveguide irradiator of 3.580 and 3.946 W/kg at 5.25 and 5.80 GHz, respectively.

#### V. Conclusions

We have developed an open-ended waveguide irradiation system for validation of the SAR measurement system and/or for E-field probe calibration in the 802.11a frequency band 5.15 to 5.825 GHz. A fourth-order polynomial least-square fit to the experimental data gives SAR variations close to the bottom surface of the phantom that are in excellent agreement with those obtained using the FDTD method. The experimentally-determined peak 1-g SARs are within 1 to 2 percent of those obtained using the FDTD numerical calculations.

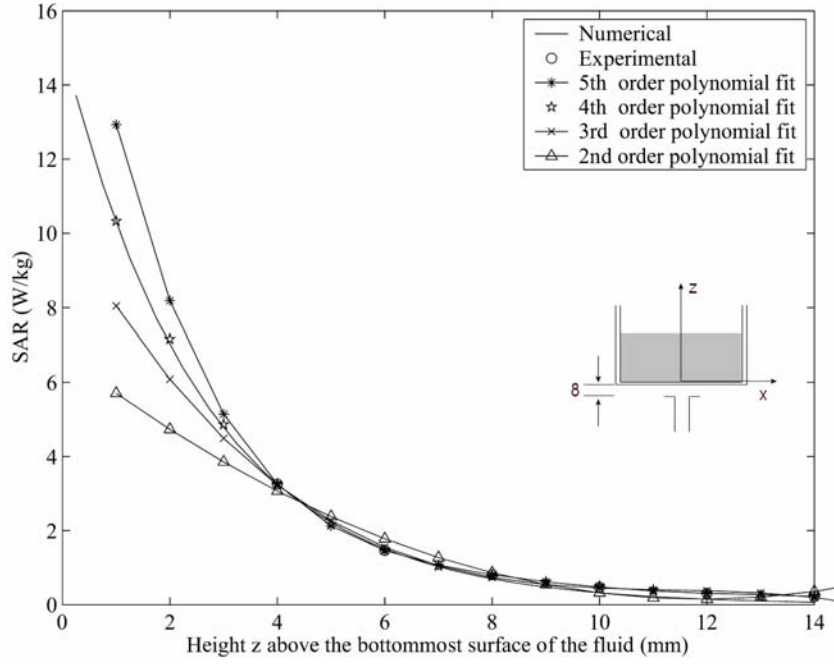


Fig. 8. Comparison of the experimentally measured and FDTD-calculated variation of the SAR with depth in the body-simulant planar phantom at 5.25 GHz. Also shown are the SARs extrapolated from experimental values to heights of 1, 3, 5, 7 and 9 mm above the bottom of the phantom using second-, third-, fourth-, and fifth-order least-square fit polynomials.

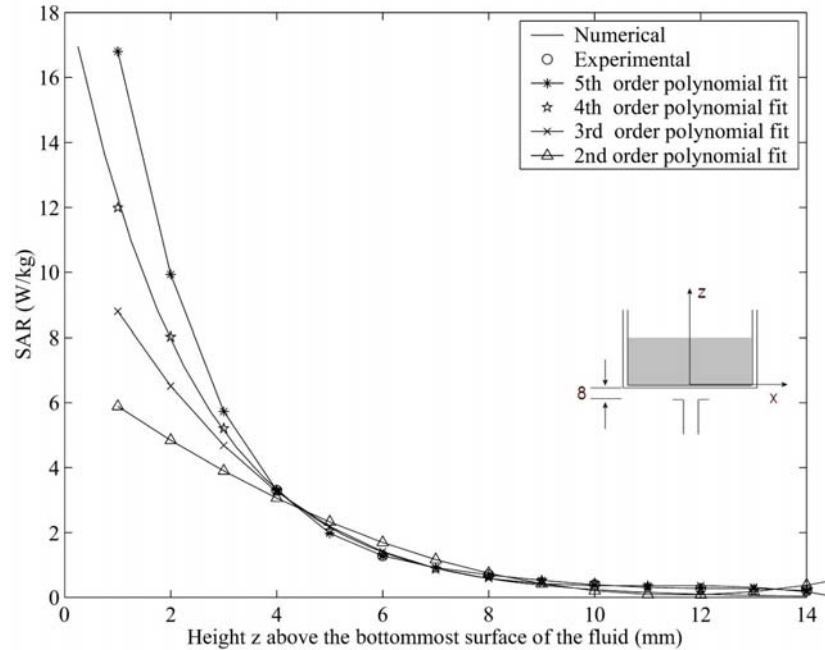


Fig. 9. Comparison of the experimentally measured and FDTD-calculated variation of the SAR with depth in the body-simulant planar phantom at 5.8 GHz. Also shown are the SARs extrapolated from experimental values to heights of 1, 3, 5, 7 and 9 mm above the bottom of the phantom using second-, third-, fourth-, and fifth-order least-square fit polynomials.

## REFERENCES

1. IEEE Std. C95.1, "IEEE Standard for Safety Levels with Respect to Human Exposure to Radiofrequency Electromagnetic Fields, 3 kHz to 300 GHz," Institute of Electrical and Electronics Engineers, Piscataway, NJ, 1999.
2. ICNIRP (International Commission on Non-Ionizing Radiation Protection), "Guidelines for limiting exposure to time-varying electric, magnetic, and electromagnetic fields (up to 300 GHz)", *Health Physics*, Vol. 74, pp. 494-522, 1998.
3. IEEE Standards Coordinating Committee 34 Draft Standard, "Recommended Practice for Determining the Peak Spatial-Average Specific Absorption Rate (SAR) in the Human Body Due to Wireless Communications Devices: Experimental Techniques," Institute of Electrical and Electronics Engineers, 2002.
4. CENELEC EN50361, "Basic Standard for Measurement of Specific Absorption Rate Related to Human Exposure to Electromagnetic Fields from Mobile Telephones (300-MHz-3 GHz), CENELEC European Committee for Electrotechnical Standardization, rue de Stassart 35, B-1050, Brussels, Belgium.
5. IEC TC 106/PT62209, "Evaluation of Human Exposure to Radiofrequency Fields from Handheld and Body-Mounted Wireless Communications Devices in the Frequency Range of 30 MHz to 6 GHz: Human Models, Instrumentation Procedures," Draft Standard in preparation, 2003.
6. U.S. Federal Communications Commission (FCC), "Additional Information for Evaluating Compliance of Mobile and Portable Devices with FCC Limits for Human Exposure to Radiofrequency Emissions," Supplement C Edition 01-01 to OET Bulletin 65 Edition 97-01, June 2001.
7. A. Taflove (Ed.), *Advances in Computational Electrodynamics: The Finite-Difference Time-Domain Method*, Artech House, Boston, MA, 1998.
8. A. Taflove and S. C. Hagness, *Computational Electrodynamics: The Finite-Difference Time-Domain Method*, Artech House, Boston, MA, 2000.
9. P. J. Dimbylow and S. M. Mann, "SAR Calculations in an Anatomically-Based Realistic Model of the Head for Mobile Communication Transceivers at 900 MHz and 1.8 GHz," *Physics in Med. And Biol.*, Vol. 39, pp. 1537-1553, 1994.
10. O. P. Gandhi and J. Y. Chen, "Electromagnetic Absorption in the Human Head from Experimental 6 GHz Handheld Transceivers," *IEEE Trans. On Electromag. Compat.*, Vol. 37, pp. 547-558, 1995.

11. M. A. Jensen and Y. Rahmat-Samii, "EM Interaction in Handset Antennas and a Human in Personal Communications," *Proc. IEEE*, Vol. 83, pp. 7-17, 1995.
12. M. Okoniewski and M. A. Stuchly, "A Study of Handset Antenna and Human Body Interaction, *IEEE Trans. On Microwave Theory and Tech.*, Vol. 44, pp. 1855-1864, 1996.
13. M. A. Stuchly and S. S. Stuchly, "Experimental Radio and Microwave Dosimetry, " in *Handbook of Biological Effects of Electromagnetic Fields*, 2<sup>nd</sup> ed., C. Polk and E. Postow, Eds. Boca Raton, FL: CRC, pp. 295-336, 1996.
14. H. I. Bassen and G. S. Smith, "Electric Field Probes – a Review," *IEEE Trans. Antennas Propagat.*, Vol. AP-31, pp. 710-718, September 1983.
15. D. Hill, "Waveguide Techniques for the Calibration of Miniature Electric Field Probes for Use in Microwave Bioeffects Studies," *IEEE Trans. Microwave Theory Tech.*, Vol. MTT-30, pp. 92-94, 1982.
16. N. Kuster and Q. Balzano, "Energy Absorption Mechanism by Biological Bodies in the Near Field of Dipole Antennas Above 300 MHz," *IEEE Trans. Veh. Technol.*, Vol. 41, pp. 17-23, February 1992.
17. M. A. Stuchly, S. S. Stuchly, and A. Kraszewski, "Implantable Electric Field Probes – Some Performance Characteristics," *IEEE Trans. Biomed. Eng.*, Vol. BME-31, pp. 526-531, July 1984.
18. C. M. Furse, Q. S. Yu, and O. P. Gandhi, "Validation of the Finite-Difference Time-Domain Method for Near-Field Bioelectromagnetic Simulations," *Microwave and Optical Technology Letters*, Vol. 16, pp. 341-345, 1997.

## APPENDIX E

### **Uncertainty Analysis**

The uncertainty analysis of the University of Utah SAR Measurement System is given in Table E.1. Several of the numbers on tolerances are obtained by following procedures similar to those detailed in [3], while others have been obtained using methods suggested in [5].

Table E.1. Uncertainty analysis of the University of Utah SAR Measurement System.

Uncertainty Component	Uncertainty Value ± %	Probability Distribution	Divisor	$C_i$ $1-g$	Standard Unc. $u_i$ ± %	$v_i$
<b>Measurement System</b>						
Probe calibration	2.0	N	1	1	2.0	$\infty$
Axial isotropy of the probe	4.0	R	$\sqrt{3}$	$(1-c_p)^{1/2}$	1.6	$\infty$
Hemispherical isotropy of the probe	5.5	R	$\sqrt{3}$	$\sqrt{c_p}$	0.0	$\infty$
Boundary effect	0.8	R	$\sqrt{3}$	1	0.5	$\infty$
Probe linearity	3.0	R	$\sqrt{3}$	1	1.7	$\infty$
System detection limits	1.0	R	$\sqrt{3}$	1	0.6	$\infty$
Readout electronics	1.0	N	1	1	1.0	$\infty$
Response time	0.0	R	$\sqrt{3}$	1	0.0	$\infty$
Integration time	0.5	R	$\sqrt{3}$	1	0.3	$\infty$
RF ambient conditions	0	R	$\sqrt{3}$	1	0	$\infty$
Probe positioner mechanical tolerance	0.5	R	$\sqrt{3}$	1	0.3	$\infty$
Probe positioning with respect to phantom shell	2.0	R	$\sqrt{3}$	1	1.2	$\infty$
Extrapolation, interpolation, & integration algorithms for maximum SAR evaluation	5.0	R	$\sqrt{3}$	1	2.9	$\infty$
<b>Test Sample Related</b>						
Device positioning	3	R	$\sqrt{3}$	1	1.7	11
Device holder uncertainty	3	R	$\sqrt{3}$	1	1.7	7
Output power variation – SAR drift measurement	5	R	$\sqrt{3}$	1	2.9	$\infty$
<b>Phantom and Tissue Parameters</b>						
Phantom uncertainty – base thickness tolerance	10.0	R	$\sqrt{3}$	1	5.8	$\infty$
Liquid conductivity – deviation from target values	0.4	R	$\sqrt{3}$	0.7	0.2	$\infty$
Liquid conductivity – measurement uncertainty	1.5	R	$\sqrt{3}$	0.7	0.6	$\infty$
Liquid permittivity – deviation from target values	0.8	R	$\sqrt{3}$	0.6	0.3	$\infty$
Liquid permittivity – measurement uncertainty	3.5	R	$\sqrt{3}$	0.6	1.2	$\infty$
<b>Combined Standard Uncertainty</b>						
<b>Expanded Uncertainty (95% Confidence Level)</b>						
		RSS			8.3	
					$\pm 16.6$	

APPENDIX F

**COARSE SCANS FOR THE HIGHEST SAR REGION FOR THE WISTRON NEWEB  
MODEL EM-500AG MINI PCI BUILT INTO ACER MODEL MS2143  
NOTEBOOK COMPUTER**

(FCC ID# NKRMS2143CM6)

**December 5, 2003**

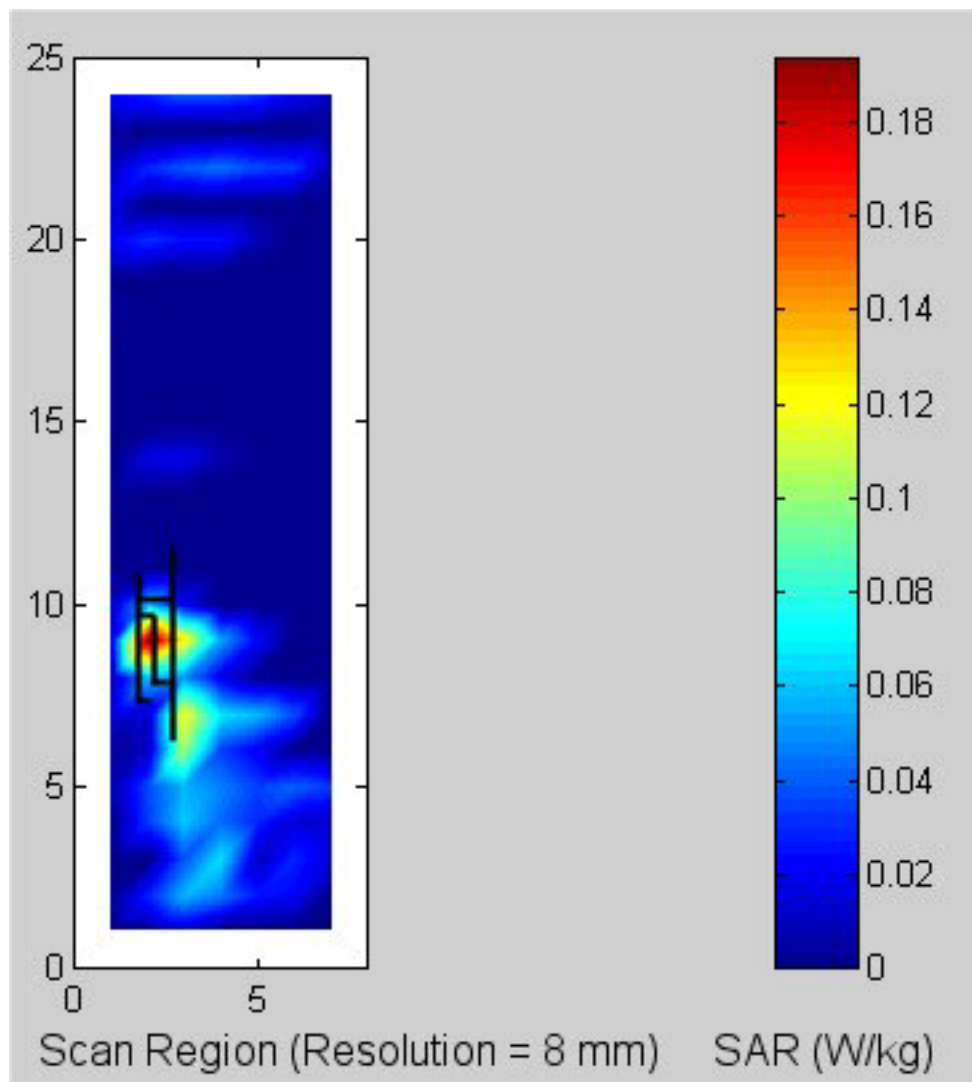


Fig. F.1. **End-on position (Configuration 3).** Coarse scan for the highest SAR region for the Wistron NeWeb Model EM-500AG right-side "Main" antenna. **Frequency = 5.26 GHz, normal mode.**

Table F.1. **End-on position (Configuration 3). Normal mode at 5.26 GHz.** The SARs measured for the Wistron NeWeb Model EM-500AG right-side "Main" antenna.

**1-g SAR = 0.173 W/kg**

**December 5, 2003**

**a. At depth of 1 mm**

0.368	0.396	0.383	0.293	0.166
0.449	0.563	0.541	0.506	0.393
0.391	0.554	0.595	0.491	0.320
0.450	0.549	0.556	0.543	0.451
0.400	0.492	0.425	0.375	0.270

**b. At depth of 3 mm**

0.173	0.190	0.179	0.150	0.100
0.208	0.260	0.276	0.254	0.189
0.205	0.261	0.285	0.254	0.191
0.218	0.272	0.293	0.280	0.221
0.196	0.225	0.219	0.186	0.131

**c. At depth of 5 mm**

0.076	0.091	0.082	0.078	0.059
0.098	0.119	0.131	0.124	0.089
0.112	0.128	0.147	0.139	0.121
0.108	0.132	0.151	0.143	0.112
0.097	0.101	0.109	0.089	0.064

**d. At depth of 7 mm**

0.036	0.051	0.042	0.045	0.036
0.056	0.066	0.063	0.066	0.047
0.071	0.080	0.099	0.091	0.088
0.064	0.071	0.083	0.081	0.070
0.053	0.052	0.056	0.045	0.035

**e. At depth of 9 mm**

0.023	0.035	0.024	0.030	0.024
0.039	0.046	0.037	0.043	0.032
0.056	0.064	0.084	0.074	0.074
0.048	0.046	0.054	0.056	0.056
0.031	0.035	0.034	0.027	0.022

December 5, 2003

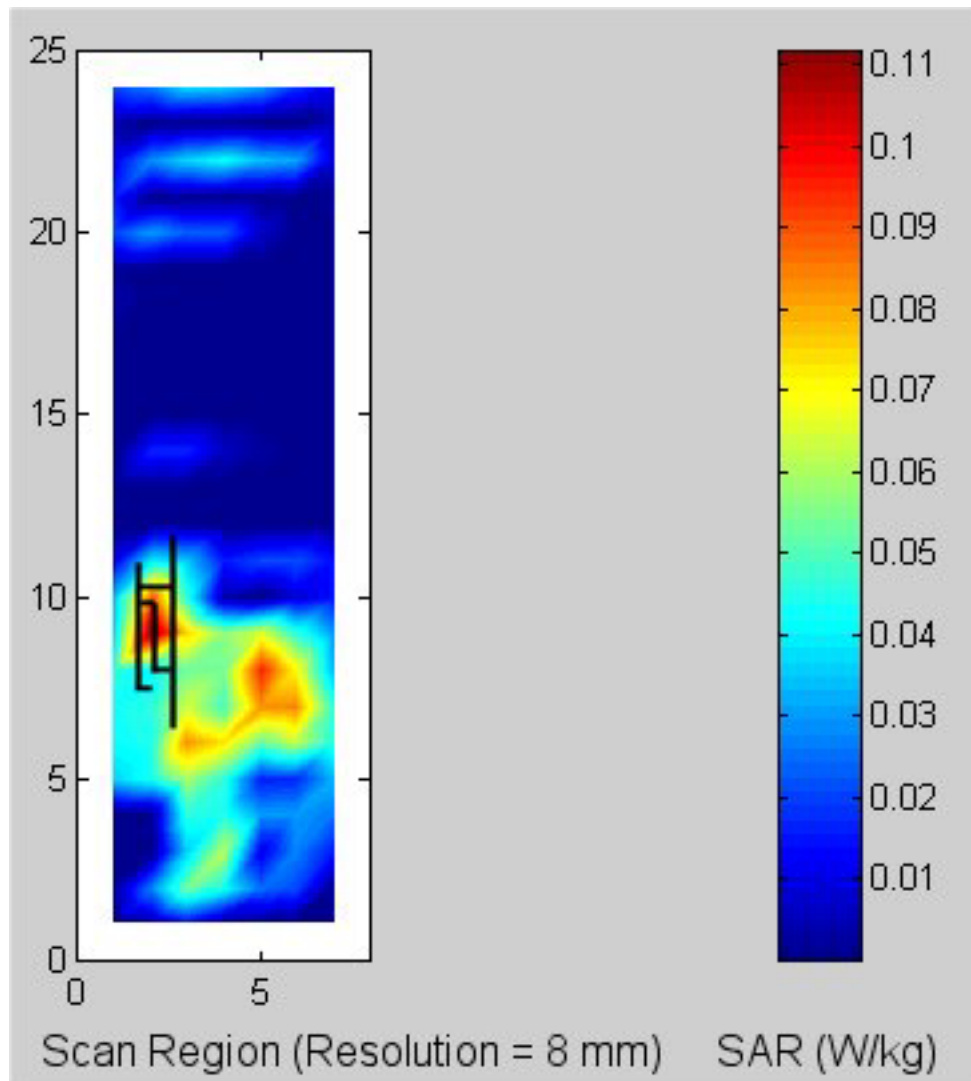


Fig. F.2. **End-on position (Configuration 3).** Coarse scan for the highest SAR region for the Wistron NeWeb Model EM-500AG right-side "Main" antenna. **Frequency = 5.745 GHz, normal mode.**

Table F.2. **End-on position (Configuration 3). Normal mode at 5.745 GHz.** The SARs measured for the for the Wistron NeWeb Model EM-500AG right-side "Main" antenna.

**1-g SAR = 0.112W/kg**

**December 5, 2003**

**a. At depth of 1 mm**

0.307	0.235	0.154	0.296	0.252
0.219	0.274	0.363	0.343	0.353
0.241	0.313	0.368	0.390	0.339
0.204	0.344	0.255	0.363	0.293
0.210	0.203	0.297	0.311	0.260

**b. At depth of 3 mm**

0.107	0.105	0.109	0.128	0.097
0.085	0.118	0.151	0.151	0.145
0.102	0.136	0.164	0.173	0.157
0.103	0.148	0.145	0.175	0.147
0.121	0.140	0.181	0.184	0.172

**c. At depth of 5 mm**

0.031	0.039	0.060	0.050	0.033
0.029	0.044	0.051	0.055	0.053
0.040	0.057	0.070	0.075	0.075
0.057	0.065	0.078	0.086	0.081
0.078	0.102	0.113	0.123	0.119

**d. At depth of 7 mm**

0.015	0.011	0.023	0.021	0.016
0.014	0.016	0.015	0.017	0.022
0.019	0.029	0.037	0.041	0.046
0.038	0.039	0.043	0.052	0.056
0.060	0.078	0.080	0.096	0.093

**e. At depth of 9 mm**

0.015	0.004	0.006	0.011	0.014
0.012	0.008	0.008	0.005	0.013
0.012	0.020	0.030	0.033	0.037
0.028	0.032	0.030	0.041	0.045
0.053	0.063	0.070	0.085	0.086

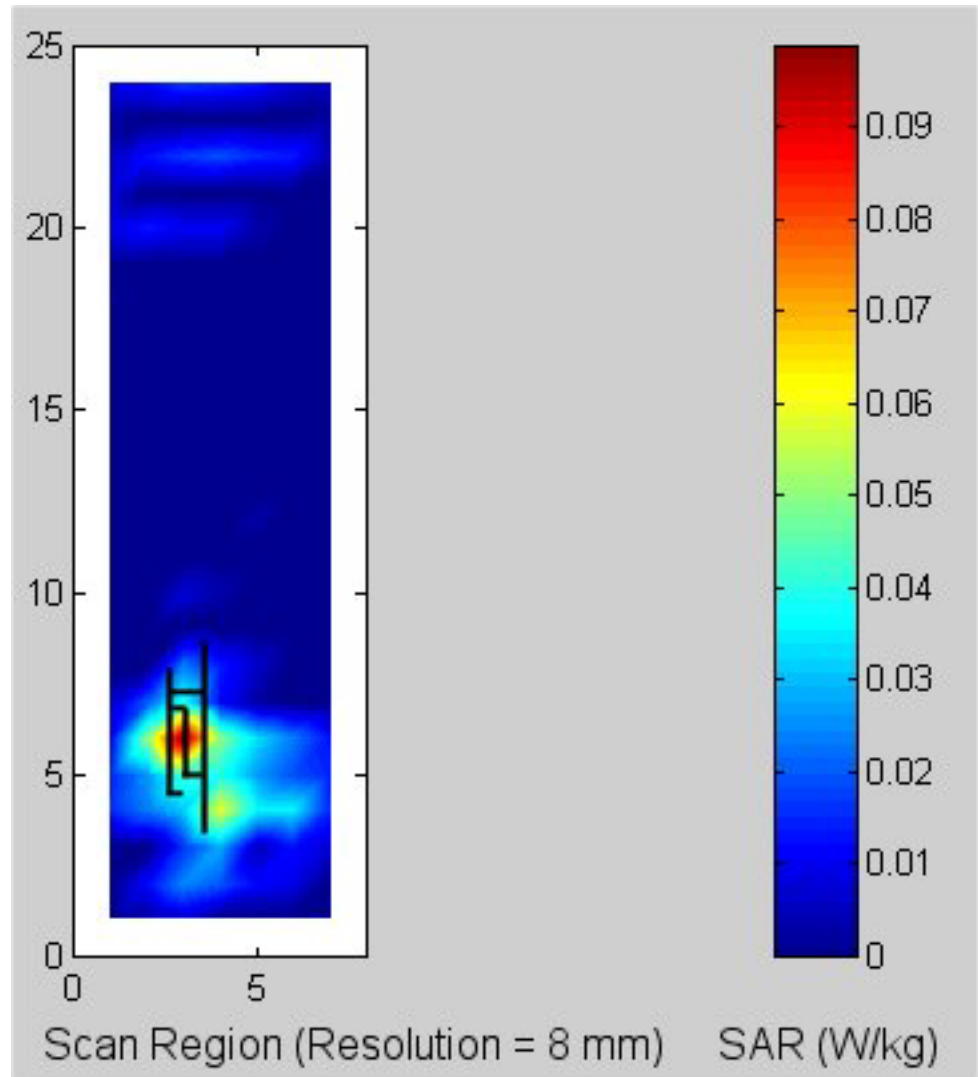


Fig. F.3. **End-on position (Configuration 3).** Coarse scan for the highest SAR region for the Wistron NeWeb Model EM-500AG right-side "Main" antenna. **Frequency = 5.805 GHz, normal mode.**

Table F.3. **End-on position (Configuration 3). Normal mode at 5.805 GHz.** The SARs measured for the Wistron NeWeb Model EM-500AG right-side "Main" antenna.

**1-g SAR = 0.089 W/kg**

**December 5, 2003**

**a. At depth of 1 mm**

0.086	0.094	0.141	0.094	0.129
0.163	0.194	0.240	0.200	0.171
0.153	0.216	0.265	0.233	0.180
0.216	0.257	0.238	0.242	0.187
0.106	0.125	0.164	0.200	0.146

**b. At depth of 3 mm**

0.066	0.056	0.081	0.074	0.077
0.090	0.088	0.120	0.105	0.092
0.090	0.125	0.143	0.133	0.119
0.104	0.114	0.133	0.131	0.110
0.086	0.088	0.085	0.120	0.092

**c. At depth of 5 mm**

0.049	0.039	0.061	0.058	0.052
0.053	0.048	0.067	0.064	0.060
0.055	0.074	0.080	0.087	0.086
0.066	0.064	0.085	0.087	0.085
0.077	0.069	0.057	0.078	0.073

**d. At depth of 7 mm**

0.038	0.033	0.057	0.045	0.043
0.039	0.037	0.049	0.051	0.050
0.040	0.050	0.053	0.067	0.065
0.060	0.054	0.064	0.070	0.075
0.070	0.058	0.048	0.057	0.064

**e. At depth of 9 mm**

0.032	0.032	0.053	0.036	0.041
0.035	0.033	0.043	0.047	0.045
0.037	0.040	0.043	0.054	0.050
0.057	0.051	0.051	0.057	0.060
0.059	0.051	0.040	0.046	0.053

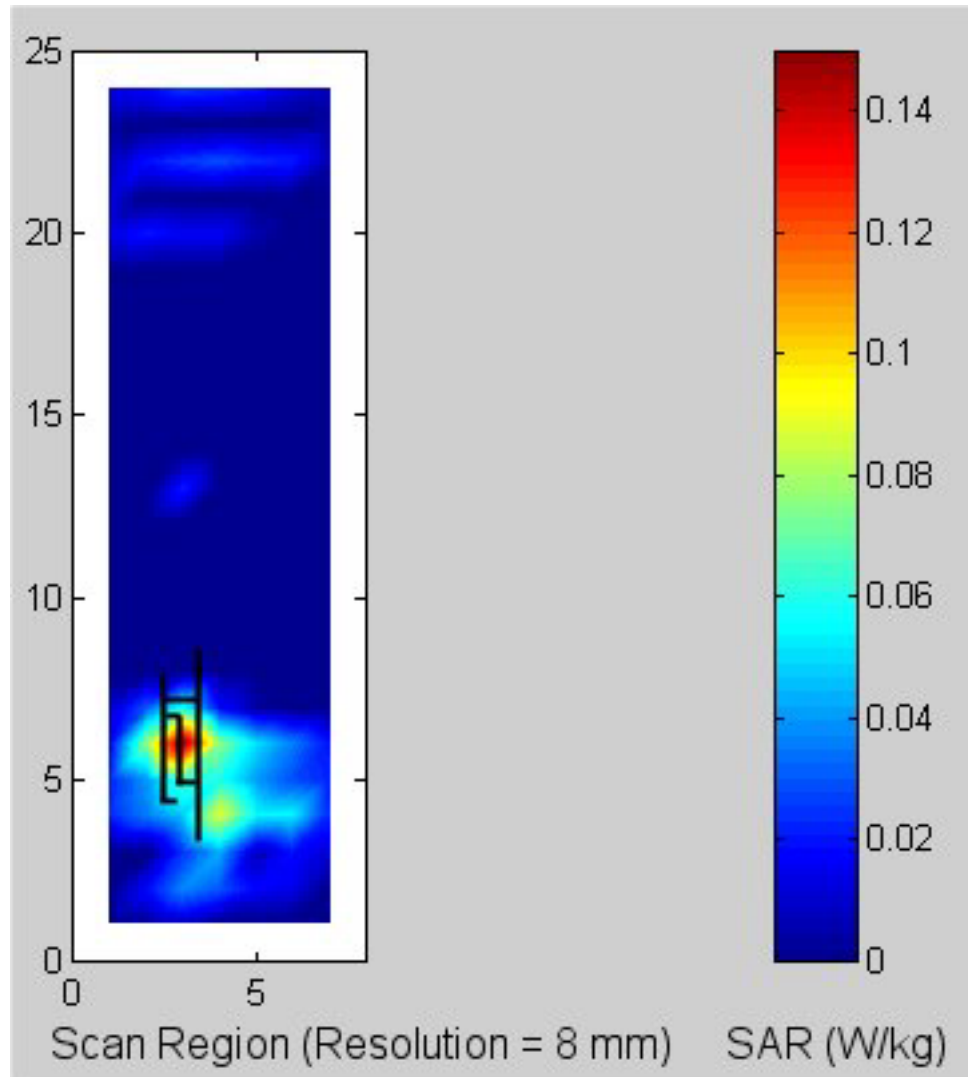


Fig. F.4. **End-on position (Configuration 3).** Coarse scan for the highest SAR region for the Wistron NeWeb Model EM-500AG right-side "Main" antenna. **Frequency = 5.25 GHz, turbo mode.**

Table F.4. **End-on position (Configuration 3). Turbo mode at 5.25 GHz.** The SARs measured for the Wistron NeWeb Model EM-500AG right-side "Main" antenna.

1-g SAR = 0.129 W/kg					December 5, 2003
<b>a. At depth of 1 mm</b>					
0.203	0.213	0.299	0.274	0.202	
0.227	0.224	0.316	0.388	0.303	
0.245	0.301	0.355	0.470	0.288	
0.296	0.256	0.425	0.444	0.349	
0.253	0.312	0.395	0.351	0.327	
<b>b. At depth of 3 mm</b>					
0.107	0.131	0.139	0.135	0.118	
0.128	0.132	0.163	0.171	0.142	
0.127	0.161	0.178	0.210	0.164	
0.143	0.143	0.206	0.215	0.200	
0.133	0.161	0.206	0.200	0.208	
<b>c. At depth of 5 mm</b>					
0.058	0.072	0.065	0.068	0.066	
0.072	0.076	0.085	0.078	0.066	
0.067	0.084	0.090	0.095	0.092	
0.067	0.078	0.101	0.109	0.113	
0.076	0.091	0.117	0.125	0.128	
<b>d. At depth of 7 mm</b>					
0.035	0.038	0.037	0.040	0.037	
0.041	0.043	0.047	0.046	0.035	
0.039	0.047	0.051	0.054	0.052	
0.035	0.043	0.058	0.069	0.067	
0.053	0.062	0.081	0.092	0.080	
<b>e. At depth of 9 mm</b>					
0.024	0.024	0.025	0.028	0.024	
0.023	0.025	0.028	0.032	0.023	
0.024	0.032	0.036	0.038	0.031	
0.023	0.028	0.040	0.056	0.045	
0.043	0.050	0.067	0.075	0.058	

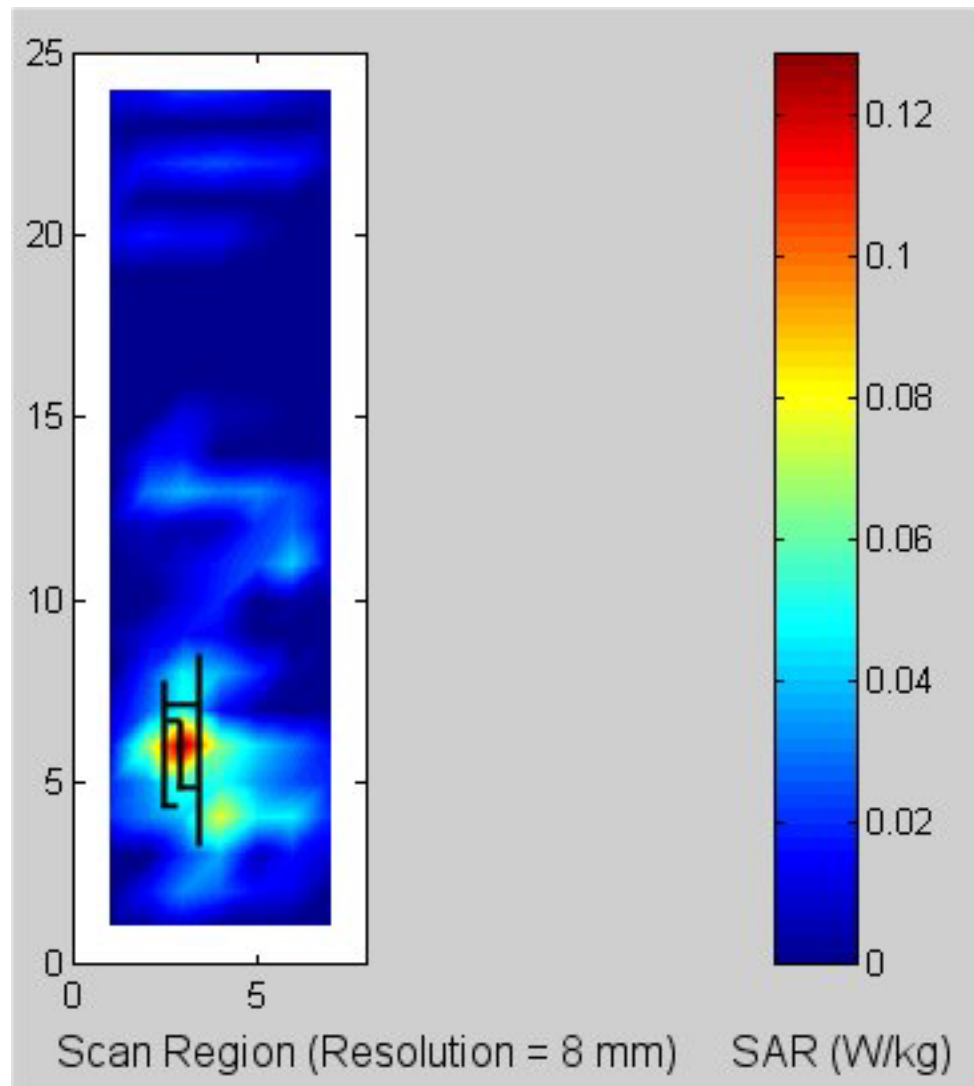


Fig. F.5. **End-on position (Configuration 3).** Coarse scan for the highest SAR region for the Wistron NeWeb Model EM-500AG right-side "Main" antenna. **Frequency = 5.76 GHz, turbo mode.**

Table F.5. **End-on position (Configuration 3). Turbo mode at 5.76 GHz.** The SARs measured for the Wistron NeWeb Model EM-500AG right-side "Main" antenna.

1-g SAR = 0.114 W/kg

December 5, 2003

**a. At depth of 1 mm**

0.133	0.143	0.210	0.201	0.230
0.220	0.192	0.234	0.182	0.291
0.284	0.198	0.306	0.371	0.200
0.160	0.284	0.295	0.311	0.247
0.199	0.147	0.232	0.215	0.183

**b. At depth of 3 mm**

0.075	0.077	0.113	0.117	0.125
0.109	0.112	0.137	0.128	0.150
0.122	0.126	0.155	0.177	0.153
0.130	0.169	0.196	0.204	0.201
0.098	0.085	0.108	0.121	0.122

**c. At depth of 5 mm**

0.047	0.042	0.059	0.069	0.064
0.057	0.071	0.086	0.092	0.085
0.060	0.083	0.098	0.101	0.114
0.109	0.124	0.151	0.151	0.172
0.051	0.054	0.051	0.067	0.085

**d. At depth of 7 mm**

0.036	0.026	0.035	0.043	0.035
0.039	0.051	0.063	0.068	0.058
0.045	0.062	0.084	0.080	0.088
0.097	0.111	0.133	0.131	0.152
0.033	0.038	0.030	0.041	0.061

**e. At depth of 9 mm**

0.030	0.019	0.030	0.028	0.027
0.036	0.043	0.053	0.053	0.045
0.042	0.054	0.082	0.073	0.073
0.092	0.108	0.125	0.128	0.137
0.027	0.026	0.024	0.032	0.043

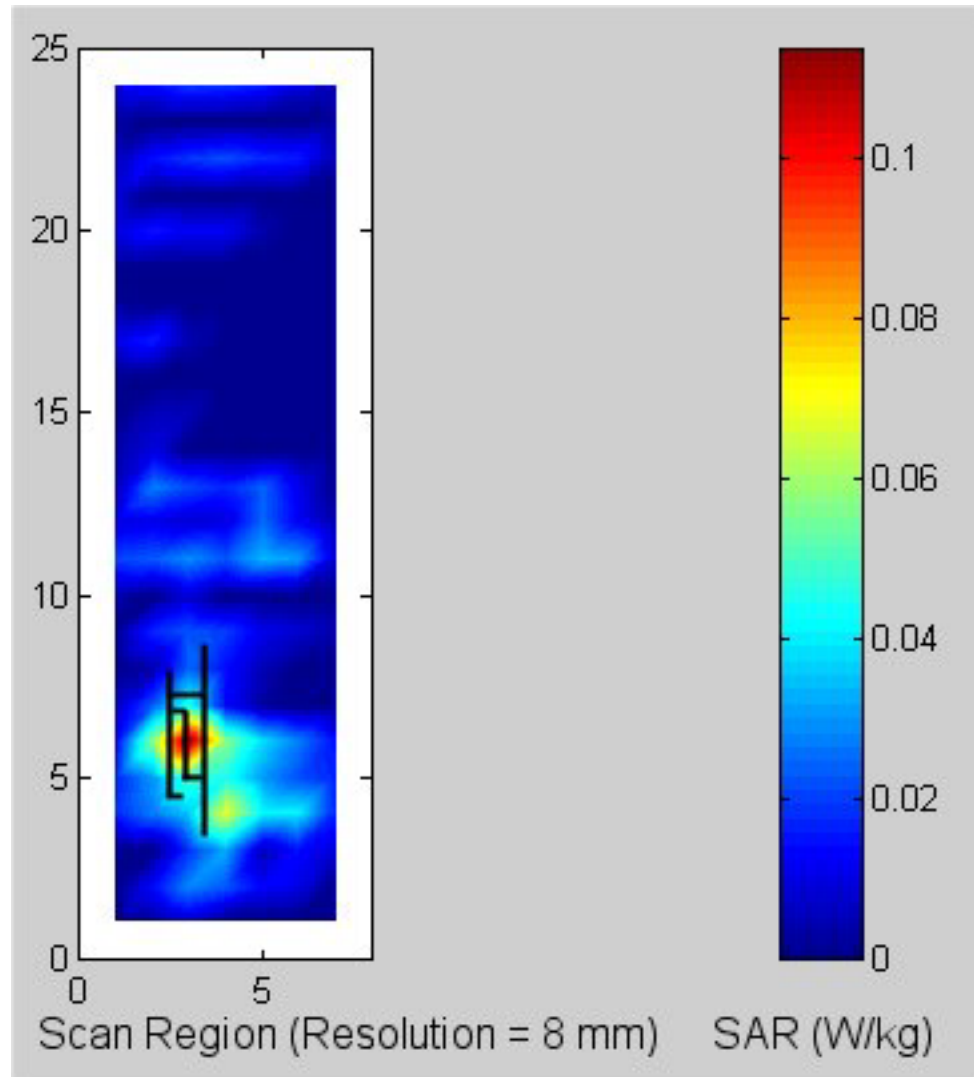


Fig. F.6. **End-on position (Configuration 3).** Coarse scan for the highest SAR region for the Wistron NeWeb Model EM-500AG right-side "Main" antenna. **Frequency = 5.80 GHz, turbo mode.**

Table F.6. **End-on position (Configuration 3). Turbo mode at 5.80 GHz.** The SARs measured for the Wistron NeWeb Model EM-500AG right-side "Main" antenna.

1-g SAR = 0.127 W/kg

December 5, 2003

**a. At depth of 1 mm**

0.246	0.187	0.216	0.254	0.219
0.304	0.270	0.323	0.212	0.235
0.259	0.243	0.229	0.259	0.186
0.237	0.282	0.324	0.258	0.191
0.151	0.299	0.272	0.255	0.252

**b. At depth of 3 mm**

0.144	0.133	0.143	0.147	0.133
0.162	0.161	0.176	0.152	0.141
0.147	0.145	0.145	0.148	0.122
0.151	0.164	0.156	0.144	0.109
0.122	0.158	0.159	0.149	0.134

**c. At depth of 5 mm**

0.092	0.099	0.097	0.089	0.086
0.099	0.109	0.109	0.105	0.095
0.092	0.099	0.098	0.098	0.087
0.103	0.107	0.093	0.088	0.075
0.104	0.103	0.104	0.107	0.087

**d. At depth of 7 mm**

0.070	0.079	0.068	0.062	0.063
0.077	0.086	0.083	0.076	0.075
0.068	0.079	0.073	0.079	0.069
0.078	0.084	0.075	0.066	0.064
0.091	0.086	0.084	0.096	0.075

**e. At depth of 9 mm**

0.062	0.068	0.050	0.052	0.055
0.072	0.076	0.073	0.065	0.067
0.059	0.068	0.060	0.071	0.062
0.069	0.076	0.069	0.061	0.062
0.080	0.080	0.079	0.095	0.071

## APPENDIX G

### VARIATION OF SAR AS A FUNCTION OF DEPTH Z IN THE LIQUID FOR LOCATIONS OF THE HIGHEST SAR (FROM TABLES F.1 TO F.6)

December 5, 2003

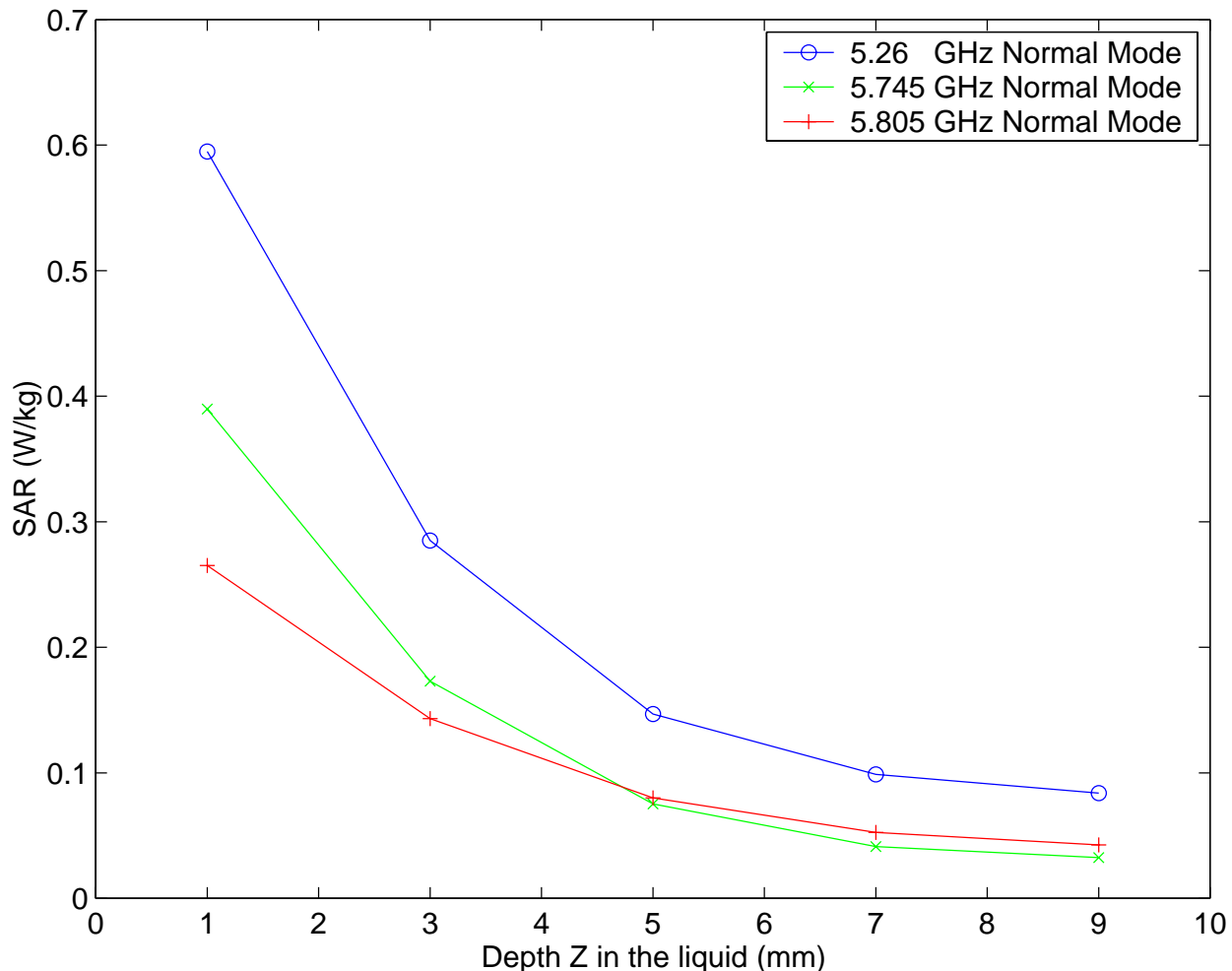


Fig. G.1. Right-side "Main" antenna End-on (Configuration 3). Plot of the SAR variation as a function of depth Z in the liquid for locations of the highest SAR for the Wistron NeWeb Model EM-500AG Mini PCI built into Acer Model MS2143 Notebook Computer (from Tables F.1 to F.3).

December 5, 2003

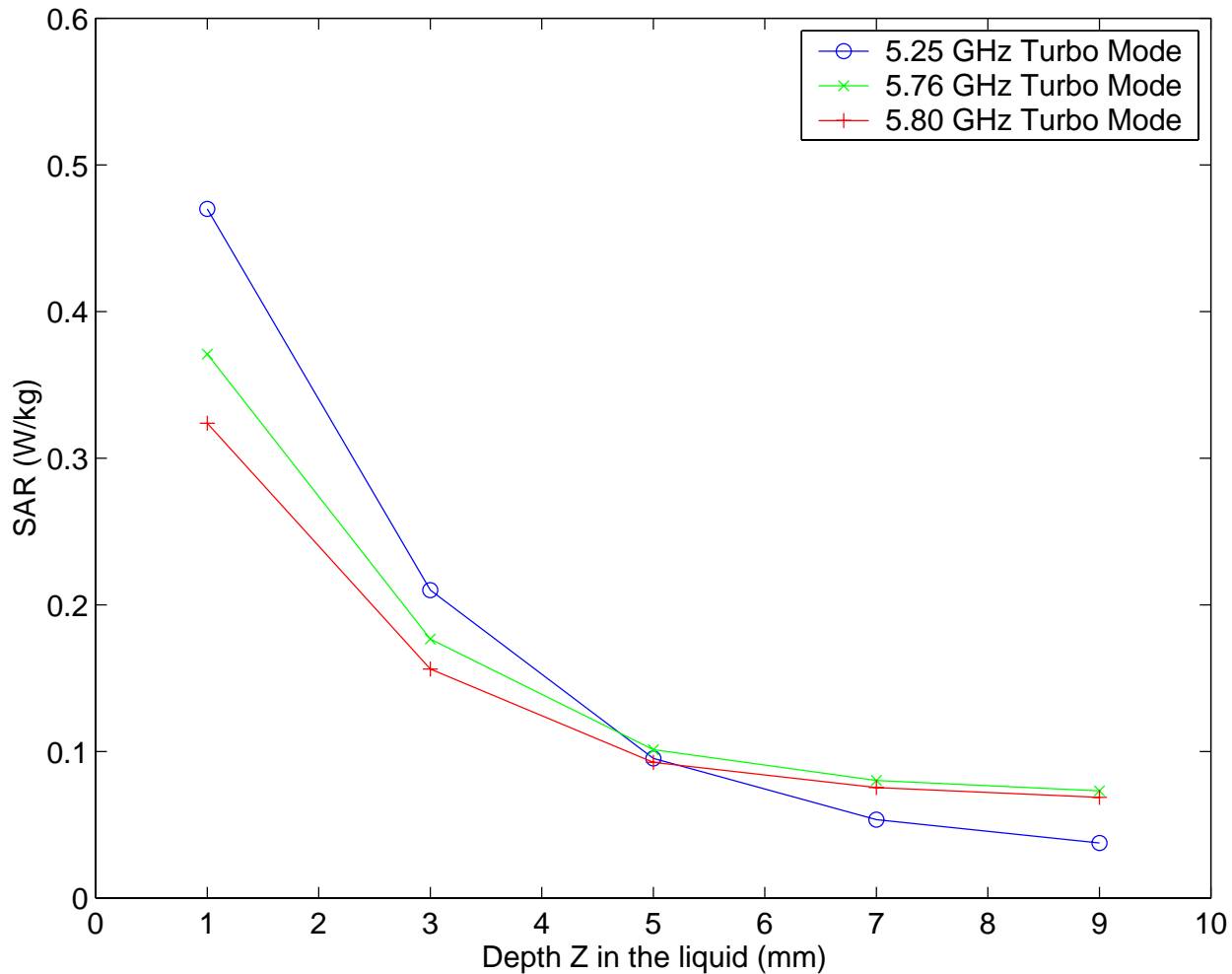


Fig. G.2. **Right-side "Main" antenna End-on (Configuration 3).** Plot of the SAR variation as a function of depth  $Z$  in the liquid for locations of the highest SAR for the Wistron NeWeb Model EM-500AG Mini PCI built into Acer Model MS2143 Notebook Computer (from Tables F.4 to F.6).